FAULT TOLERANT CONTROL OF PMSM WITH INTER-TURN SHORT CIRCUIT FAULT

A Dissertation

by

JIAYUAN ZHANG

Submitted to the Office of Graduate and Professional Studies of
Texas A&M University
in partial fulfillment of the requirements for the degree of

DOCTOR OF PHILOSOPHY

Chair of Committee,	Merhdad Ehsani
Co-Chair of Committee,	Wei Zhan
Committee Members,	Hamid A. Toliyat
	Shankar P. Bhattacharyya
Head of Department,	Miroslav M. Begovic

May 2019

Major Subject: Electrical Engineering

ABSTRACT

Due to its high-torque density and high efficiency, the Permanent Magnet Synchronous Motor (PMSM) is widely used in a broad range of applications. Extensive work has been presented in the literature related to modeling, fault diagnosis and fault tolerant (FT) control of electric drive system. On the other hand, because of higher requirements in industry, higher performance is always expected with implementation of new structure, new fault detection and new control method. In this background, the author proposed diagnosis method with a novel objective, identification of fault degree instead of fault isolation. Based on this concept, a new FT control based on fault degree information is proposed to optimize post-fault performance. The diagnosis and FT control can be applied on PMSM with inter-turn short circuit (SC). Its theoretical base and practical performance are presented and its strength over previous methods are come up with.

ACKNOWLEDGMENTS

CONTRIBUTORS AND FUNDING SOURCES

NOMENCLATURE

SC   short circuit

PMSM   permanent magnet synchronous motor

FT   fault tolerant

FOC   field oriented control

HMM   hidden Markov model

TABLE OF CONTENTS

LIST OF FIGURES

viii

LIST OF TABLES

1. INTRODUCTION AND LITERATURE REVIEW

1.1 Background

PMSMs are widely used in industry thanks to their compactness, high efficiency and high dynamic performances. According to a market research, PMSM Market is expected to garner $31.1 billion by 2022, registering a CAGR of 10.9% during the forecast period 2016-2022. Major factors influencing the PMSM market growth are rising need and demand for energy-efficient low power-consuming motors, growing demand of PMSMs in industrial and agricultural sectors, and increasing awareness towards the use of green vehicles. Furthermore, increasing emphasis on the maintenance and use of standard motors is likely to create opportunities for PMSM market growth in the future.

The major application include: automation, consumer electronics, automotive & transportation, lab equipment, medical, military and aerospace.

High reliability is necessarily required for some applications. Thereby, great efforts have been put on its fault. Generally, research in this area can be broadly classified into three major categories: 1. how to accurately and effectively modeling the PMSM with fault or the fault on its performance; 2. fault detection of different types of fault; 3. when fault happens, how to implement fault control.

On the other hand, due to increase complexity and requirements in industry, although well-studied, all of above areas are constantly advancing to following this new trend.

1.2 Purpose of Thesis

The main objective of this thesis is to propose a method that can improve the performance when inter-turn SC occurs in PMSM. In this thesis, a new FT control is proposed to reduce the torque ripple if fault happens. On the other hand, this thesis also explore the possibility to extract more fault information instead of fault type with diagnosis.

To the best knowledge of the author, the main contributions of the work presented in this thesis can be summarized as follows:

-Studying and building model of PMSM with inter-turn SC.

-Coming up with diagnosis of this specific fault.

-Proposing FT control to improve performance. The method is verified in experiments.

1.3 Thesis Outline

This thesis is constituted by six chapters, a list of references and six appendices. In the Chapter 2, previous work in this area will be introduced, including modeling, fault detection and FT control. Chapter 3 will introduce how the new FT control is proposed and its theoretical derivation will be presented. Chapter 4 presents the verification from both simulation and experiment of FT control. Chapter 5 will introduce the author's effort on diagnosis of PMSM. Finally, chapter 6 will conclude the thesis and propose the future work to be done.

2.   OVERVIEW OF SC IN ELECTRIC MOTOR

2.1   Introduction

This work focuses on the inter-turn SC fault, which are among the most common faults in PMSMs, 30% to 40% [1]. The physical structure of inter-turn SC fault can refer to Fig. 2.1[2]. Fig.2.2 shows the circuit model built based on Fig. 2.1. Previous research in this area can be summarized in three different fields, including modeling, fault detection and FT control. Research review indicates that the previous major work is on modeling and fault detection.
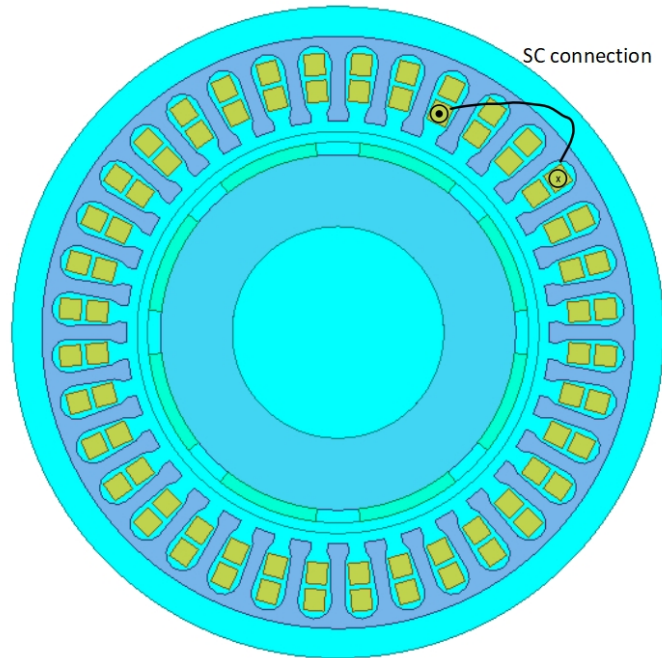
Figure 2.1: Physical representation of inter-turn SC

2.2   Modeling of PMSM with Fault

Previous research [2, 3, 4, 5, 6, 5] research on how to model PMSM with inter-turn SC. Bon-Gwan Gu in [2] modeled both series and parallel winding connections considering saliency effect.
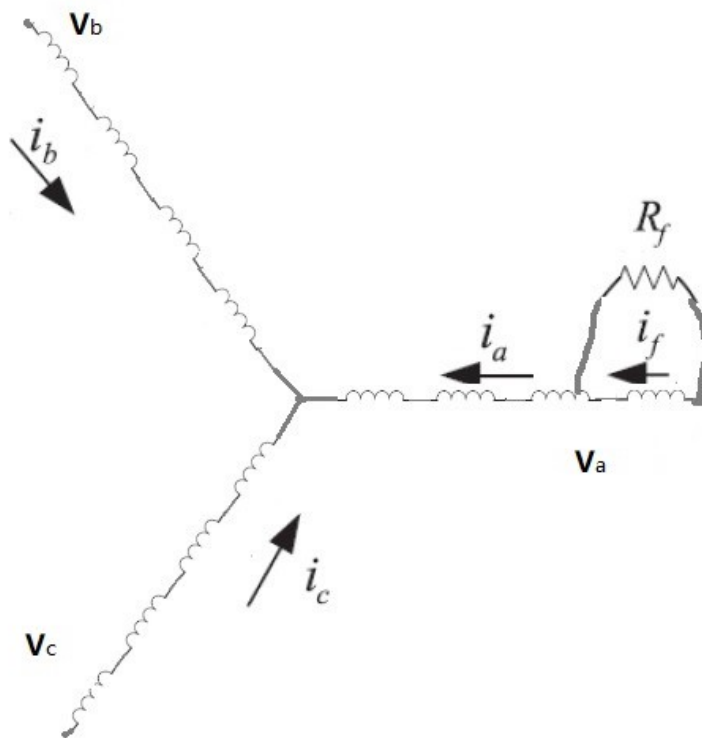
Figure 2.2: Circuit model of inter-turn SC

Ilsu Jeong et al.[3] considered the variations in inductance and back EMF term to reflect the internal turn short into the dynamics. Babak Vaseghi et al.[4] proposed analytical expressions for calculation of faulty machine inductances from healthy machine parameters. Luis Romeral et al.[5] deals with spatial harmonics due to a nonsinusoidal rotor permanent magnet configuration in the developed model. Babak Vaseghi et al.[6] proposed a simple dynamic model and validate the fault model for different levels of fault severity.

It may be noted that some also study fault detection and FT control together. In author's opinion, it may be more meaningful to model with a certain objective instead of pure modeling, considering the fact that motor is a complex electro-magnetic-mechanic component, leading to great complexity in modeling. If a certain objective is determined, some factors can be simplified to consider major factors.

2.3 Diagnosis of PMSM with Fault

Previous research [7, 8, 9, 10, 11, 12, 13, 14] focus on fault detection. Methods can be broadly classified into model-based and statistics-based. Olaf Moseler et al. [7] proposes a parameter estimation technique for fault detection on this type of motor simply by measuring the motor's input and output signals. Comparing the nominal with the computed parameters, faults can be detected. Chengning Zhang et al. [8] analyzes the influences of short circuit fault on the magnetic field and various parameters of motors and extracts feature vector for detecting inter-turn short circuit fault. J. Rosero et al. [9] investigated the relationships between stator-current-induced harmonics by means of Fourier (FFT) and discrete Wavelet Transforms (DWT) and found that Fourier Fast Transform allows detecting short circuit fault. Seung-Tae Lee et al. [10] proposed a diagnosis technique of ITF using variations of back electromotive force generated in detection coils in BLDC motors not requiring spectral analysis and complicated computation. Sergio M. A. Cruzd et al. [11] escribes the use of the Extended Park's Vector Approach (EPVA) for diagnosing the occurrence of stator winding faults in operating three-phase synchronous and asynchronous motors by the identification of a spectral component at twice the fundamental supply frequency. Bhaskar Sen et al. [12] proposes a novel method of interturn fault detection based on measurement of pulsewidth modulation (PWM) ripple current. Thierry Boileau et al. [13] implemented fault detection by comparing the magnitude of the control voltage second harmonic, derived using a proper time-domain transformation, to a predefined threshold. Hyeyun Jeong et al. [14] proposed a fault indicator calculated by introducing negative-sequence components for an early stage interturn short-circuit fault diagnosis.

It is also worthwhile to note that identification of fault degree are not studied in above work. Within this context, fault degree refers to SC percentage μ_{sc} and fault resistance r_f shown in Fig. 2.2 [2] together termed as fault degree. Identification of fault degree has two distinct advantages over fault detection. First, it provides more useful information of fault, which positively contributes to decision on how to deal with the fault. For example, if the fault is serious and aggravates quickly, it is better to stop it instead of further operation, while FT control can be applied if it is a minor

fault. Besides, information of fault degree can be helpful to reconfiguration of the controller and achievement of optimized FT control. The second advantage will be explicitly shown in this work.

It is worthwhile to mention that identification of this specific fault degree has been researched before. H. Nakamura et al. [15] researched on how to apply HMM for diagnosis of SC fault in induction motor. It has the drawback that fault resistance is ignored in identification of fault degree. As validated in [4], the effect of fault resistance on fault features is not negligible. In [16], it is verified by estimating the value of turn ratio and insulation resistance after different severity of inter-turn SC fault. However, it relies on certain circuit topology to eliminate the effect of common-mode voltage in single dc power supply application. B. G. Gu [17] estimates the value of turn ratio and insulation resistance by parameter estimation. As a typical model-based method, it can be used to compare with statistics-based method proposed here in the perspective of amounts and complexity of calculation.

2.4 Challenge in FT Control

In the perspective of diagnosis, more information about the fault are required. For example, how serious the fault is is concerned if the fault happens and how long it will take until the complete failure. On the other hand, more information about the fault is critical and valuable to the FT control. If the fault is minor, the motor can be still in use, while it has to be shut down if the fault is serious. Furthermore, more information about the fault can be helpful in reconfiguring the controller and achieving optimized fault tolerant control. Most previous work do not go further on FT control.

In addition to diagnosis, new method of FT control is also proposed corresponding to the diagnosis proposed. In [18], common methods of FT control are summarized as following

1. Electric machine with redundant structure

2. Additional legs of inverter, specially applied to fault of converters, not the machine itself.

3. Modification of control

Considering the additional cost incurred, the last one is preferred most times.

As for objectives of FT control, safety, output performance and cost are always mostly con-

cerned under faulty condition.

1. Safety mainly includes moderate power dissipation in the form of heating, deceleration of the propagation of the fault and extend the machine's post-fault life span.

2. Output performance requires acceptable torque ripple, speed ripple, power loss and maximally output torque capability is retained.

3. Last but equally important, minimum cost is expected.

As each coin has two sides, there is always conflict between safety and output performance. For example, Jorge G et al. in [1] proposed field weakening control to reduce fault current and decelerate the propagation of fault with ignorance of output torque capability and torque ripple. Which factor weights more is dependent on application and requirement of motor and no universal solution exists when it comes to FT control.

Taken performance into consideration, the most common and intuitive method is to discard the faulty phase to achieve symmetry in remaining phases [19, 20, 21]. However, it does not take into torque ripple and torque capability is severely impaired as a result of discarding one phase winding. On the contrary, it is intuitive to think of the question whether the faulty phase can be kept with minor fault. The main advantage is that the output capability will be less affected and pressure of load can be shared by 3 phases instead of 2 phases. I. Jeong et al. [3] does keep the faulty phase and reduces the torque ripple meanwhile by elimination of negative component of current in the controller. However, it necessarily relies on two conditions to make FT it work. First, it requires fault resistance to be negligible. Besides, it overlooks the side effect of fault current on torque.

A solution that can solve torque ripple issue while maintaining fault phase is expected. Thereby, the author proposed a new method in following chapters.

3. NEW FT CONTROL

The original idea is whether the FT control can be optimized with more information of fault. The side effect of keeping faulty phase has to be taken into consideration. One effect is possible severe fault incurred caused by operation of faulty phase winding. Another effect is the inevitable torque ripple. The proposed method in this work is to solve the torque ripple issue.

3.1 Analysis of Torque Ripple

To solve the torque ripple issue, the question will show up how the torque ripple is generated. To understand it, the operation of healthy PMSM is presented in Fig. 3.1. This figure shows that healthy PMSM supplied with 3-phase balanced current will generate constant torque. However, if faulty PMSM is still supplied with 3-phase balanced current, torque ripple will be generated. Fig. 3.2 clearly shows how it happens. Due to the additional circuit loop, the fault current i_f is generated, leading current through the winding being SC not equal to supplied phase current anymore. Thereby torque ripple is generated.
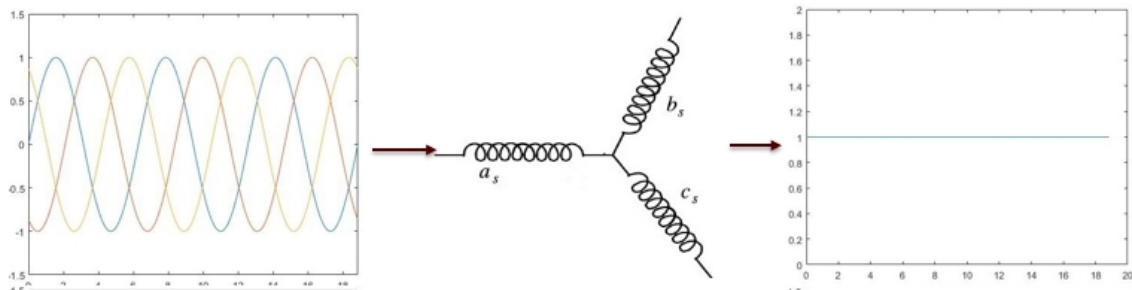
Figure 3.1: Healthy PMSM case

However, it should be clear that Fig. 3.2 is not the real case when fault happens. Most times, PMSM is controlled in a closed-loop system, imbalancing 3-phase current if fault happens. In the simulation section, the resulted 3-phase current will be displayed.
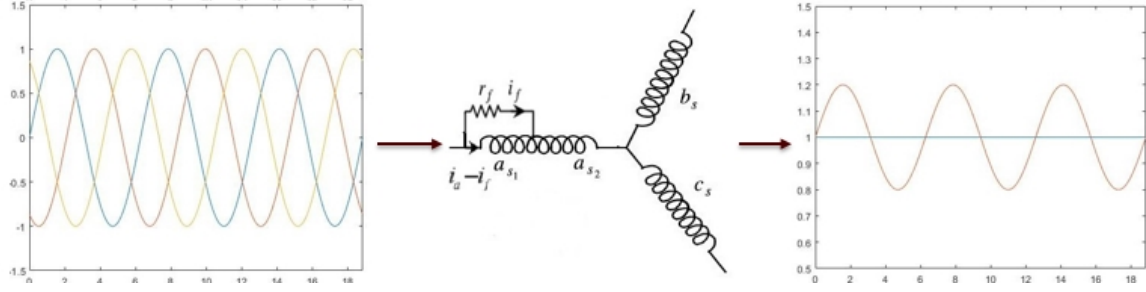
Figure 3.2: Faulty PMSM case

On the other hand, it can also be understood in pure mathematical view. Equation 3.1 shows the torque of healthy PMSM, while equation 3.2 shows the torque of faulty PMSM. In this perspective, fault current i_f is responsible for torque ripple.

$$Torque = f(i_{abc}) \tag{3.1}$$

$$Torque = f(i_{abc}, i_f) \tag{3.2}$$

3.2 Derivation of New FT Control

Analyzing the cause of torque ripple cannot directly solve the issue, considering the fact fault current i_f cannot be removed. However, an original idea comes up that if 3-phase balanced current cannot generate constant torque, can 3-phase unbalanced current generate constant torque since PMSM has asymmetrical winding structure? This is the main idea of following work in FT control. In this section, the author seeks to prove the existence of such unbalanced current and find it.

There are several constraints to be met in derivation. The first one is the sum of 3-phase current equal to 0, since no neutral lines in most PMSM. The equation is shown in equation 3.3. The second one comes from the application of Kirchhoff's voltage law on the SC loop, as shown in equation 3.4. This equation considers the voltage drop due to self-inductance, mutual inductance and resistance and back EMF. It relates fault current with phase current.

$$i_a + i_b + i_c = 0 \tag{3.3}$$

9

$$i_f r_f = (i_a - i_f)R_{as1} + L_{as1}\frac{d(i_a - i_f)}{dt} + e_{as1} + M_{as1,2}\frac{di_a}{dt} + M_{as1,b}\frac{di_b}{dt} + M_{as1,c}\frac{di_c}{dt} \quad (3.4)$$

Equation 3.5 is the output torque equation based on power conservation.

$$Torque = \frac{i_a e_a + i_b e_b + i_c e_c - i_f e_{as1}}{\omega_{mech}} \quad (3.5)$$

With substitution of equation 3.6-3.9, equation 3.5 can be simplified as equation 3.11. This is the very equation revealing the essential relationship between instantaneous current and instantaneous torque if SC ratio μ_{sc} is known.

$$e_a = K\omega_{mech}sin(\theta) \quad (3.6)$$

$$e_b = K\omega_{mech}sin(\theta - \frac{2\pi}{3}) \quad (3.7)$$

$$e_c = K\omega_{mech}sin(\theta + \frac{2\pi}{3}) \quad (3.8)$$

$$e_{as1} = \mu_{sc}e_a \quad (3.9)$$

$$\mu_{sc} = \frac{N_{as1}}{N_{as}} = \frac{R_{as1}}{R_{as}} \quad (3.10)$$

$$Torque = K(i_a sin(\theta) + i_b sin(\theta - \frac{2\pi}{3}) + i_c sin(\theta + \frac{2\pi}{3}) - i_f \mu_{sc}sin(\theta)) \quad (3.11)$$

Combining equation 3.3, 3.4 and 3.11, there are 3 independent equations. Assume torque is the desired torque and thereby is known. Besides, assume the rotor position angle θ and machine parameters are known. Then four variables are left unknown, including i_f and i_{abc}. When the number of equations is less than the number of unknown variables, solutions usually exist. However, in this case, it involves first-order differential equation. Therefore, it is too early to claim the existence of solution.

On the other hand, an alternative option is to find a solution satisfying all above constrains. Then two new issues come up. First, how to solve equation 3.3, 3.4 and 3.11. Another practical issue is how to implement the possible solution into motor control system. The author proposes

a solution that the FT control can be combined with existing FOC scheme. FOC will be briefly introduced in next section considering consistency.

Appendix.D shows a complete scheme of FOC. It is a closed-loop speed control. The PI controller circled generates reference of i_{sq}, or reference of torque based on equation 3.12. Inverse Park's and Clarke's transformation and SVPWM are used to generate gating signals to inverter with the ultimate goal of generating reference of i_{sq}. In other words, if i_{sq} is supplied to the PMSM, a certain torque is output.

$$Torque = \psi_f i_{sq}^* \tag{3.12}$$

On the other hand, if all currents in the PMSM are decomposed as shown in Fig. 3.3, 3.4 and 3.5 and the resulting torque is the superposition of all torque component, that is, a constant torque. Then FT control is effectively integrated with existing FOC. If all above conditions are met, a desired constant torque can still be the output.
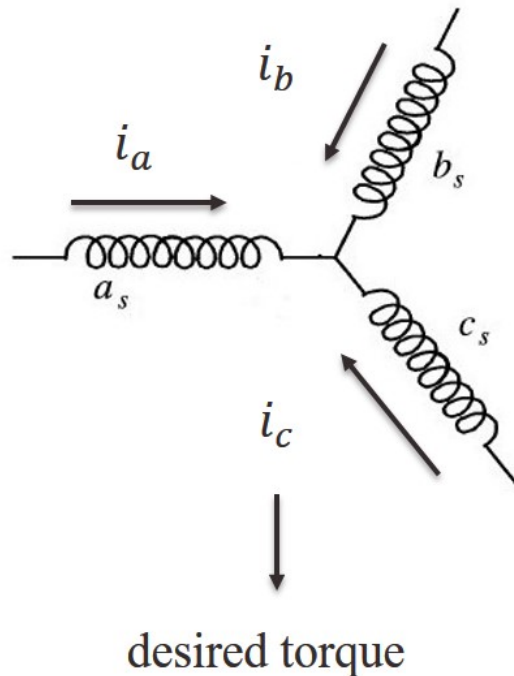
Figure 3.3: Only current generated by FOC and no fault current
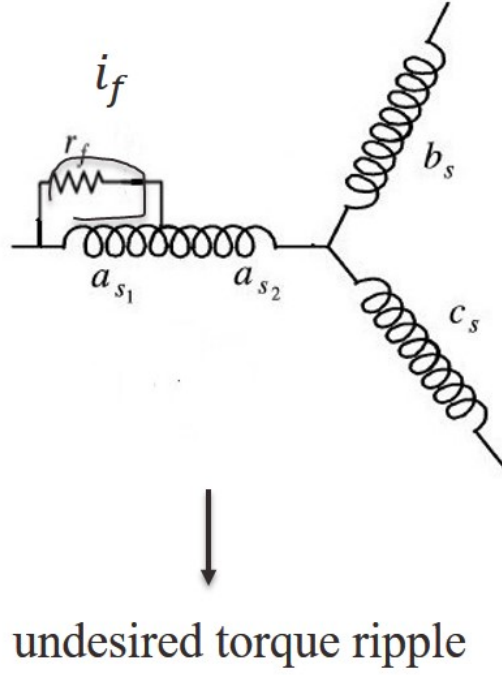
Figure 3.4: Only fault current

The new FOC scheme is shown in Fig. 3.6. The closed-loop speed control and speed PI controller are reserved, while SVPWM is discarded since 3-phase winding is not symmetrical. Instead, hysteresis control is used. The new scheme raises a new question how to derive the unknown component.

The author proposes the modified current reference shown in equation 3.13-3.15 with assumption of SC fault in phase A. The first right term in each equation is the current component generated by original FOC, while the second right term is the additionally injected current. It obviously satisfies equation 3.3.

$$i_a^{*'} = i_a^* - 2i_0 \tag{3.13}$$

$$i_b^{*'} = i_b^* + i_0 \tag{3.14}$$

$$i_c^{*'} = i_c^* + i_0 \tag{3.15}$$

Substituting equation 3.13-3.15 into equation 3.11, equation 3.16 is derived. The first right

12
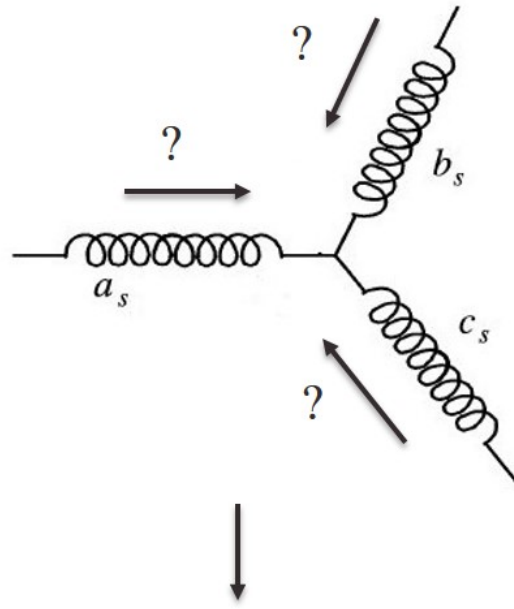
Figure 3.5: Only additionally injected current
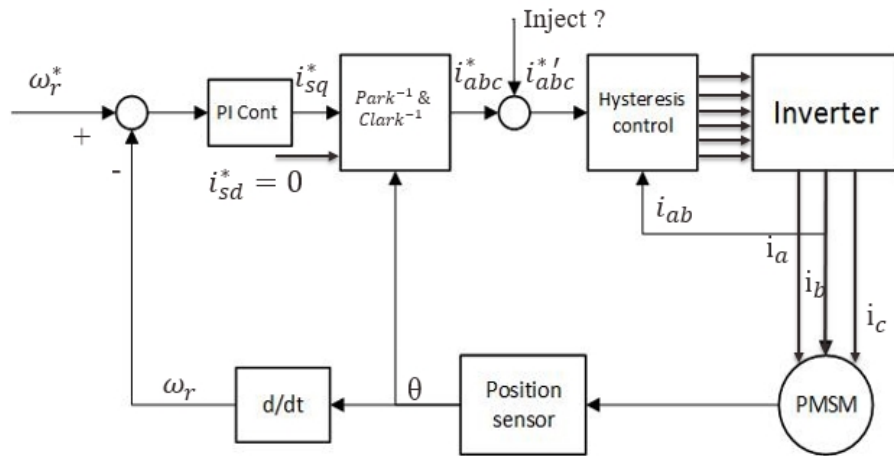
Figure 3.6: Modified FOC scheme

term is constant if FOC is used to supply 3-phase balanced current. To make the torque the desired torque with FOC, the second term can be set 0. If the second right term is 0, equation 3.17 is derived.

$$Torque = K(i_a^* sin(\theta) + i_b^* sin(\theta - \frac{2\pi}{3}) + i_c^* sin(\theta + \frac{2\pi}{3})) + K(-3i_0 - i_f \mu_{sc}) \tag{3.16}$$

$$i_f = -\frac{3}{\mu_{sc}} i_0 \tag{3.17}$$

If assuming equation 3.18:

$$i_0 = I_0 sin(\theta + \varphi_0) \tag{3.18}$$

then equation 3.19:

$$i_f = -\frac{3}{\mu_{sc}} I_0 sin(\theta + \varphi_0) \tag{3.19}$$

Applying inverse Clark's transformation and substituting equation 3.18 into equation 3.13-3.15, equation 3.20-3.22 is derived as following

$$i_a^{*'} = i_{sq}^* sin(\theta) - 2I_0 sin(\theta + \varphi_0) \tag{3.20}$$

$$i_b^{*'} = i_{sq}^* sin(\theta - \frac{2\pi}{3}) + I_0 sin(\theta + \varphi_0) \tag{3.21}$$

$$i_c^{*'} = i_{sq}^* sin(\theta + \frac{2\pi}{3}) + I_0 sin(\theta + \varphi_0) \tag{3.22}$$

Substituting equation 3.19-3.22 into equation 3.4, again assuming all machine parameters including fault degree are known, then only one unknown variables i_0. A solution is guaranteed in following format in equation 3.23 and 3.24. A closed-form solution is in Appendix.B. Solving i_0 means solving the additionally injected current.

$$I_0 = f_1(R, L, K, speed, \mu_{sc}, r_f, i_{sq}^*) \tag{3.23}$$

$$\varphi_0 = f_2(R, L, K, speed, \mu_{sc}, r_f, i_{sq}^*) \tag{3.24}$$

14

3.3 FOC

3.3.1 Introduction

In order to achieve better dynamic performance, a more complex control scheme needs to be applied to control the PM motor. With the mathematical processing power offered by the micro-controllers, advanced control strategies can be implemented, which uses mathematical transformations in order to decouple the torque generation and the magnetization functions in the PM motors. Such decoupled torque and magnetization control is commonly called rotor flux oriented control, or simply FOC [22].

3.3.2 The Main Philosophy Behind the FOC

For all types of control, the magnetic flux and produced torque should be decoupled for maintaining linearity between input and output and for achieving high dynamic drive. In the case of AC machines, the dynamic models are nonlinear and more complex than those in DC machines.

Overcoming this difficulty became possible by using space vector representations of AC machines. The flux oriented control methods allow representation of the mathematically complication AC machine in a similar manner to DC machines for obtaining control linearity, decoupling, and high performance of AC drives [23]. The main idea can be expressed in equation 3.12. You can control the torque by controlling the torque component of stator current vector.

3.3.3 Space Vector Definition

The three-phase voltages, currents, and fluxes of the AC-motors can be analyzed in terms of complex space vectors. With regard to the currents, the space vector can be defined as follows. Assuming that i_a, i_b, i_c are the instantaneous currents in the stator phases, the complex stator current vector i_s defined by:

$$i_s = i_a + \alpha i_b + \alpha^2 i_c \tag{3.25}$$

where $\alpha = e^{j\frac{2}{3}\pi}$. Fig. 3.7 shows the stator current complex space vector [22].
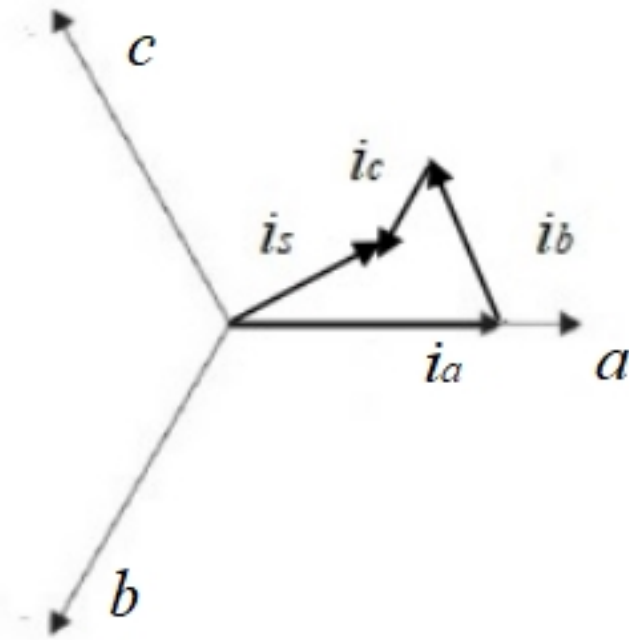
Figure 3.7: Stator Current Space Vector and Its Component in (a,b,c)

3.3.4 Clarke Transformation

The Clarke transformation is used to transform from abc reference to $\alpha\beta$ reference as shown in Fig. 3.8.

$$i_{s\alpha} = i_a \tag{3.26}$$

$$i_{s\beta} = \frac{2}{\sqrt{(3)}}i_b - \frac{2}{\sqrt{(3)}}i_c \tag{3.27}$$

3.3.5 Park Transformation

The Park transformation is used to transform from stationary $\alpha\beta$ reference to arbitrary rotating dq reference as shown in Fig. 3.9.

$$i_{sd} = i_{s\alpha}cos\theta + i_{s\beta}sin\theta \tag{3.28}$$

16
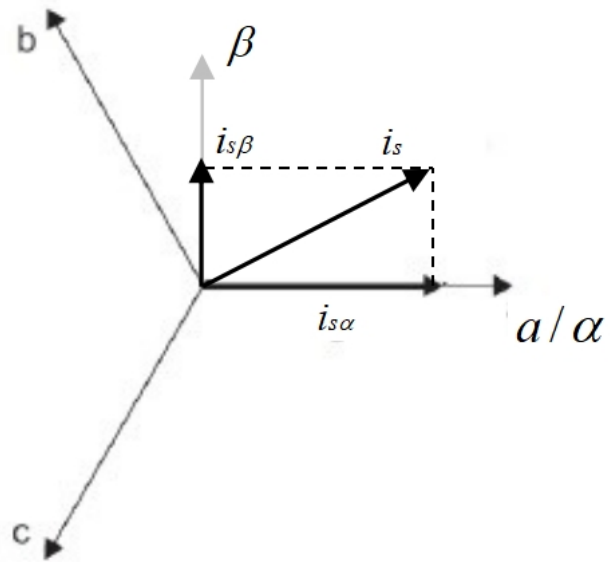
Figure 3.8: Vector in abc and $\alpha\beta$ reference

$$i_{sq} = -i_{s\alpha}sin\theta + i_{s\beta}cos\theta \tag{3.29}$$
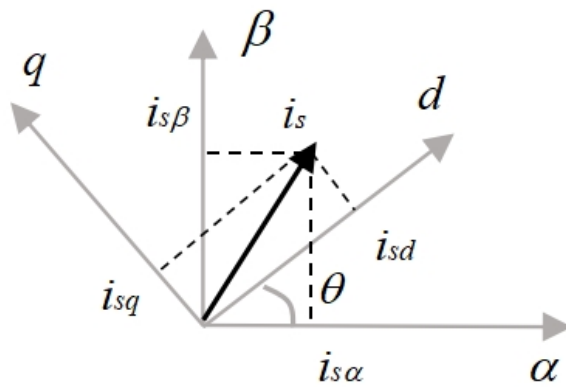
Figure 3.9: Vector in dq and $\alpha\beta$ reference

3.4 Summary

In this section, the function of i_0 is summarized as following. First, it satisfies the constraint of sum of 3-phase current equal to 0. More importantly, the modified 3-phase reference current will lead to i_f so that i'_{abc} and i_f together produce a constant torque.

On the other hand, FOC is still kept in the way that desired torque is generated by FOC and the closed-loop speed control is kept.

And it is possible that the format shown in equation 3.13-3.15 is not the only solution. However, it is at least one of the best solution in the way that torque ripple in theory is eliminated. This is why other solutions are not pursued.

Another aspect that have to be mentioned is the required information. It relies on the information not only in normal PMSM parameters, but also the fault information including not measurable L_1 and r_f, which is a possible obstacle. Chap. 5 will present a method to solve this issue.

4. SIMULATION AND EXPERIMENTAL RESULTS

The PMSM used in experiments is non-salient and has 4 pole pairs, double layer winding and 36 stator slots. Other specifics of PMSM can refer to Appendix.A. The simulation model is built based on this PMSM.

4.1 Modeling of PMSM and Inter-turn SC

Modeling PMSM has been well-researched, so does modeling PMSM with inter-turn SC. Although minor difference may exist in previous work on modeling SC, a simple circuit model of SC is widely accepted as shown in Fig. 4.1. In this model, self-inductance, resistance and back EMF are taken into consideration.
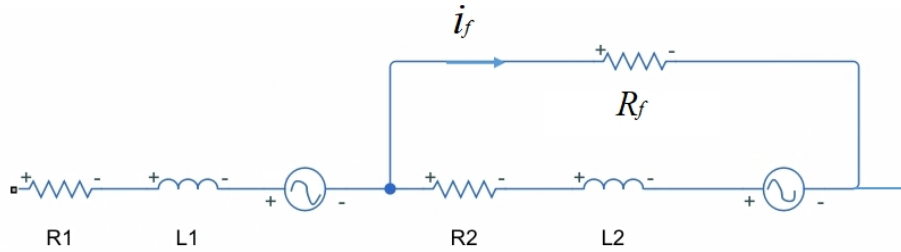
Figure 4.1: Circuit model of faulty phase winding

Besides, the mutual inductance between the winding in SC (u_2) and the winding not in SC (u_1) also take effect. In experiment, these parameters can be measured. However, the mutual inductance in equations 4.1 and 4.2 cannot be measured, and reasonable assumptions have to be used.

$$M_{a1b} = M_{a1c} = \mu_{sc}M_{ab} \tag{4.1}$$

$$M_{a2b} = M_{a2c} = (1 - \mu_{sc})M_{ab} \tag{4.2}$$

Equations 4.3-4.8 provide the equation-based modeling of PMSM with inter-turn SC. Equa-

tions 4.3-4.7 are built based on circuit model and equation 4.8 is the torque equation.

$$V_{an} = (i_a - \mu_{sc}i_f)R_s + L_1\frac{di_a}{dt} + L_2\frac{d(i_a - i_f)}{dt} + M\frac{di_b}{dt} + M\frac{di_c}{dt} + K\omega_e sin(\theta_e) \quad (4.3)$$

$$V_{bn} = i_bR_s + L_s\frac{di_b}{dt} + M\frac{di_a}{dt} + M\frac{di_c}{dt} + K\omega_e sin(\theta_e - \frac{2\pi}{3}) \quad (4.4)$$

$$V_{cn} = i_cR_s + L_s\frac{di_c}{dt} + M\frac{di_a}{dt} + M\frac{di_b}{dt} + K\omega_e sin(\theta_e + \frac{2\pi}{3}) \quad (4.5)$$

$$i_fR_f = (i_a - i_f)R_{as1} + L_{as1}\frac{d(i_a - i_f)}{dt} + e_{as1} + M_{as1,2}\frac{di_a}{dt} + M_{as1,b}\frac{di_b}{dt} + M_{as1,c}\frac{di_c}{dt} \quad (4.6)$$

$$i_a + i_b + i_c = 0 \quad (4.7)$$

$$Torque = \frac{i_a e_a + i_b e_b + i_c e_c - i_f e_{as1}}{\omega_{mech}} \quad (4.8)$$

Equation 4.9 is circuit equations expressed in matrix form.

$$
\begin{bmatrix} V_{as1} \\ V_{as2} \\ V_{bs} \\ V_{cs} \end{bmatrix} = \begin{bmatrix} R_{a1} & 0 & 0 & 0 \\ 0 & R_{a2} & 0 & 0 \\ 0 & 0 & R_s & 0 \\ 0 & 0 & 0 & R_s \end{bmatrix} \begin{bmatrix} i_{as} \\ i_{as} - i_f \\ i_{bs} \\ i_{cs} \end{bmatrix} + \begin{bmatrix} e_{as1} \\ e_{as2} \\ e_{bs} \\ e_{cs} \end{bmatrix} + \\
\begin{bmatrix} L_{a1} & M_{a1a2} & M_{a1b} & M_{a1c} \\ M_{a1a2} & L_{a2} & M_{a2b} & M_{a2c} \\ M_{a1b} & M_{a2b} & L_s & M_s \\ M_{a1c} & M_{a2c} & M_s & L_s \end{bmatrix} \frac{d}{dt} \begin{bmatrix} i_{as} \\ i_{as} - i_f \\ i_{bs} \\ i_{cs} \end{bmatrix} \quad (4.9)
$$

And if equation 4.10 is substituted into equations 4.3-4.8, the model will be reduced to model of healthy PMSM.

$$\mu_{sc} = 0; i_f = 0; L_1 = L_s; M_{a12} = 0 \quad (4.10)$$

4.2 Simulation Results

The simulation is performed in Simulink. The simulation setup is shown in Appendix.E. The PMSM is modeled based on equations 3.3-3.8. A block is used to simulate load and a block is used to model voltage source and inverter. The controller, especially in FT mode, is worthwhile of attention.

What is insider the controller is shown in Fig. 4.2. In the FT mode, a closed-loop speed control is still employed to generate i_{sq}^*, whom torque is proportional to in FOC. With application of inverse Park and Clarke transformation, reference of 3-phase current i_{abc}^* can be derived. This current superimposed with additionally injected current is the modified reference of 3-phase current. With hysteresis control, the controller will provide required gate driving signals.
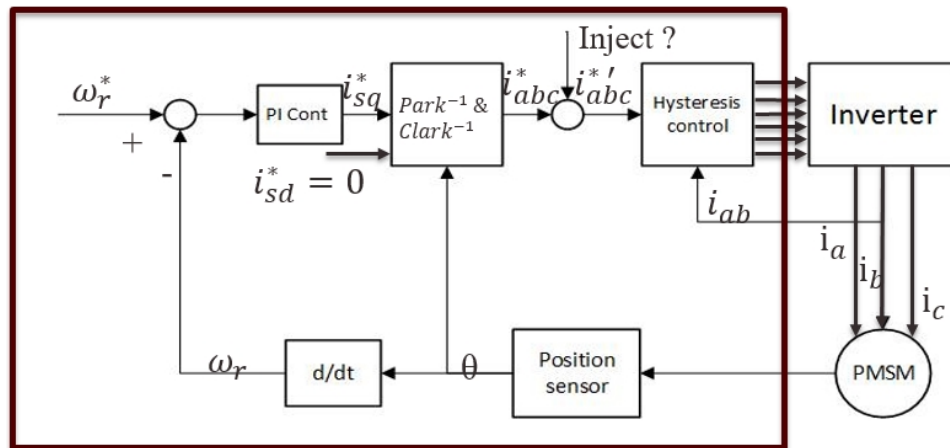
Figure 4.2: Controller in simulation

The SC is set as $\mu_{sc} = 0.145, r_f = 0.4\Omega$ in phase A, which is the same as experimental SC. The reference speed is 110rpm. For comparison of normal operation (0-0.3s), SC happened without FT control (0.3-0.5s) and SC happened with FT control (0.5-0.8s), variables in different case are plotted in the same figure as shown in Fig. 4.3-4.6. Fig. 4.3 shows the 3-phase current, it can be found that 3-phase current are not balanced since SC happens with/without FT control. To

clearly display the unbalanced 3-phase current, the amplitude of current is zoomed in in Fig. 4.4.

Fig. 4.5 shows the comparison of calculated fault current in the controller and measured fault current in the PMSM. The close match after 0.5s indicates FT control indirectly has control over fault current. Fig. 4.6 displays the torque curve, starting low torque ripple, then obvious torque ripple, finally return to low torque ripple with around 89% torque ripple reduction, leading to the conclusion that FT control does reduce the torque ripple.
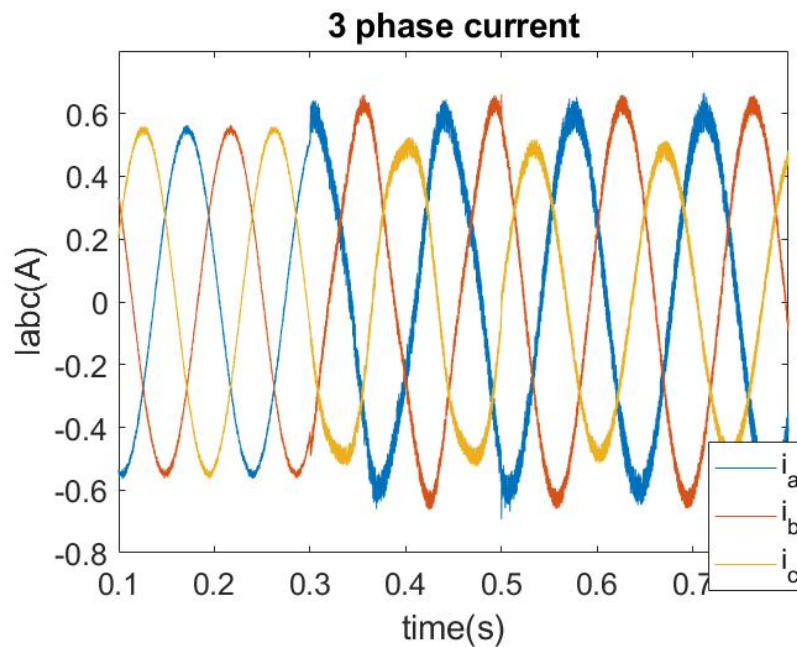
Figure 4.3: 3-phase current in simulation

Fig. 4.7 displays the torque curve simulated in the reference speed 500 rpm. The torque ripple is obviously increased, but the FT can still reduce it.

4.3 Sensitivity Analysis

Simulation results are based on the condition that all PMSM parameters are known. However, fault parameters in practice are unknown and can only be estimated with certain methods (introduced in next Chapter). These fault parameters can be classified into two categories: fault
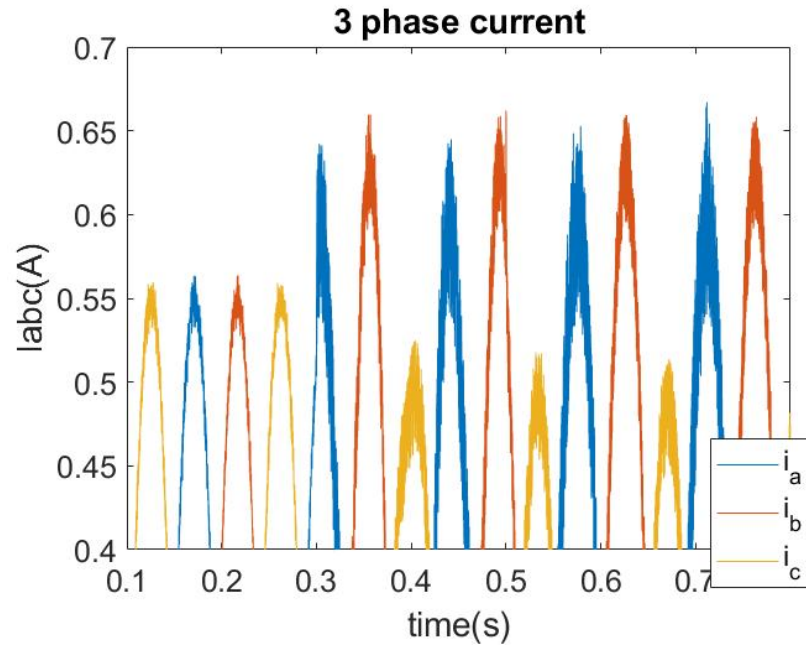
Figure 4.4: 3-phase current zoomed in
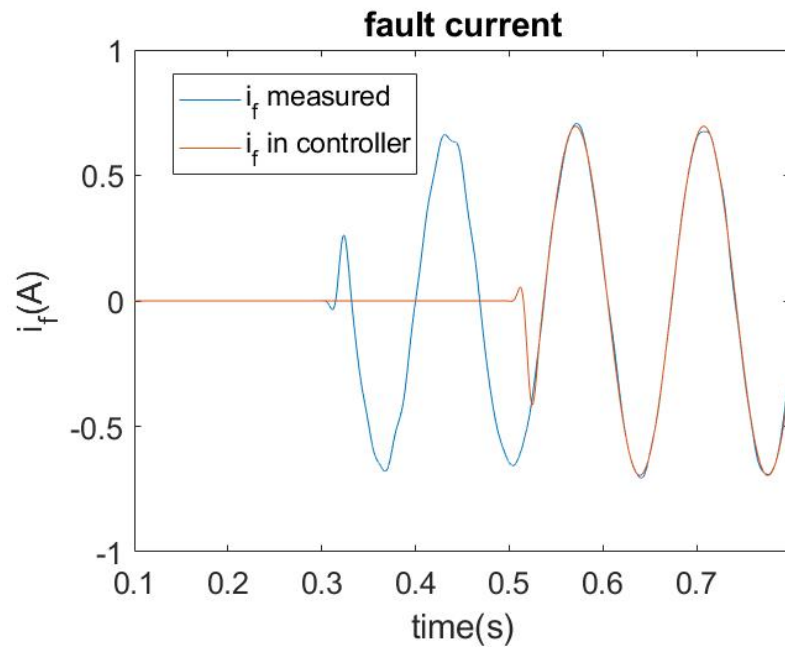
Figure 4.5: Fault current measured and calculated in simulation
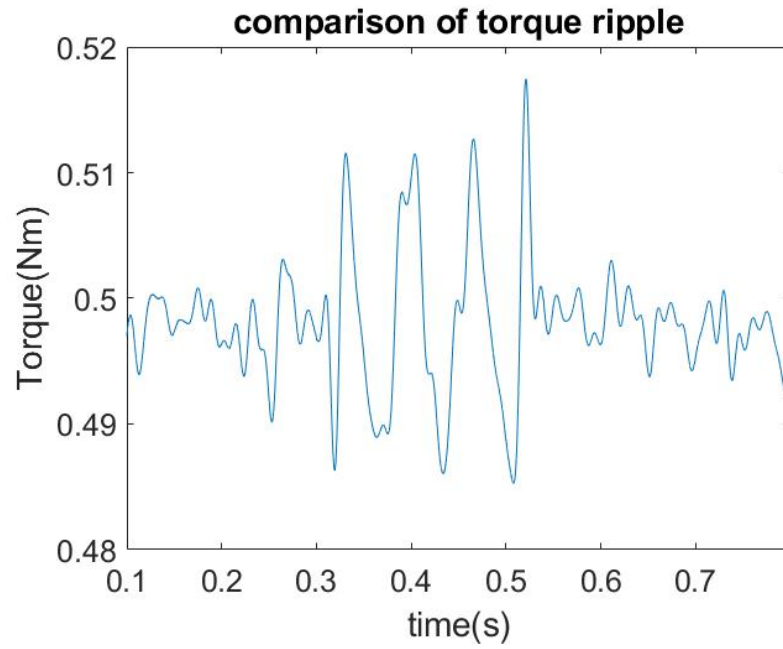
Figure 4.6: Torque in simulation
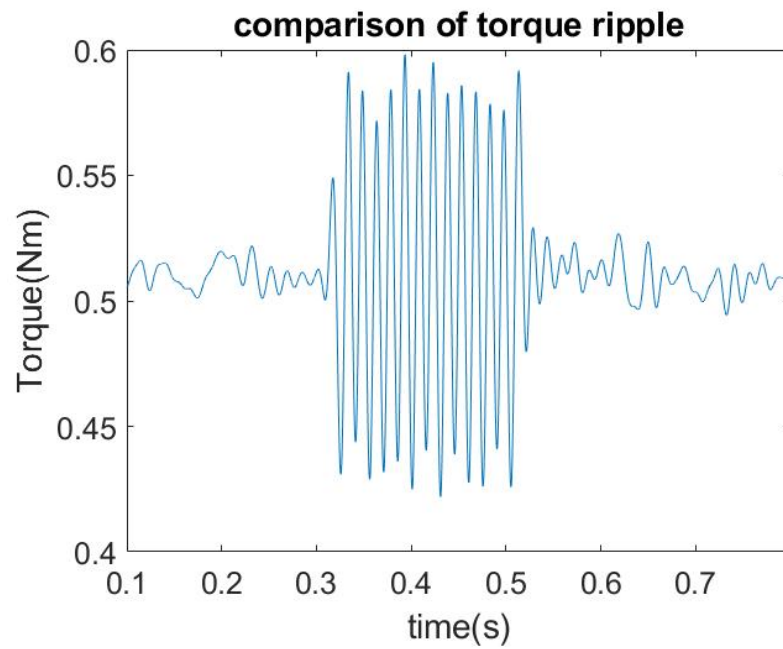
Figure 4.7: Torque in simulation

resistance r_f and SC ratio μ_{sc}, since all inductance value related with SC can be solely determined by μ_{sc}. Take the L_{a2} as an example. Its relationship with μ_{sc} can refer to Appendix. C.

If the fault parameters can only be estimated, a question arises whether the accuracy of estimated fault parameters affect the torque ripple. To answer this question, sensitivity analysis is performed both in simulation shown in Fig. 4.8 and 4.9. The x axis is the estimation error. The y axis is the SC parameters. The z axis is ratio of the torque ripple with FT control to the torque ripple without FT control.
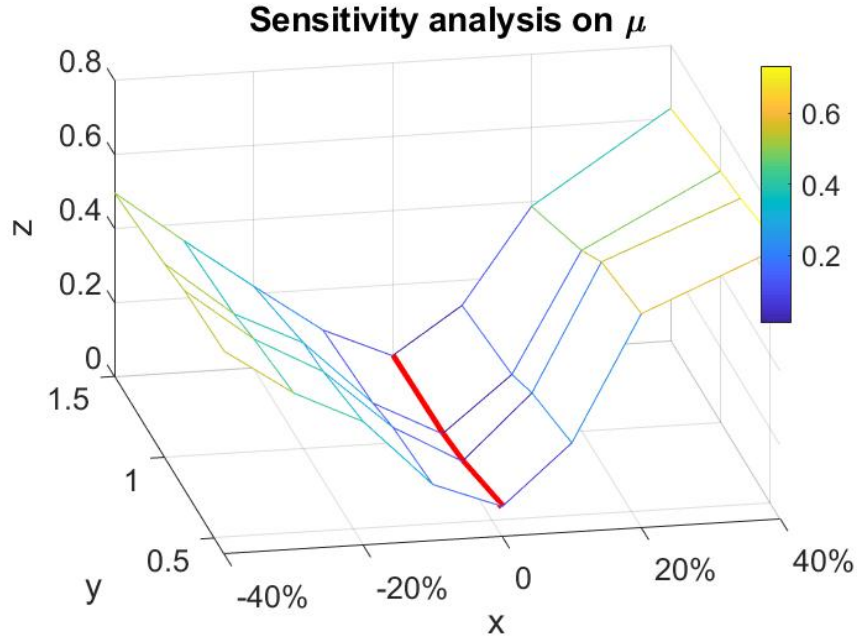
Figure 4.8: Sensitivity analysis of SC ratio

Based on these figures, following information can be determined: 1. The better the estimation is, the lower torque ripple will be. The best estimation is marked with red line as lowest torque ripple. 2. If the estimation is so bad that FT control may result in higher torque ripple than no FT control, then proposed FT control should not be used. In other words, sensitivity analysis provides a range of estimation of fault parameters where FT control can reduce the torque ripple.

To understand the 3d figure, 2d figure is plotted by fixing the fault degree as $\mu_{sc} = \frac{0.4}{2.75}$ $r_f =$
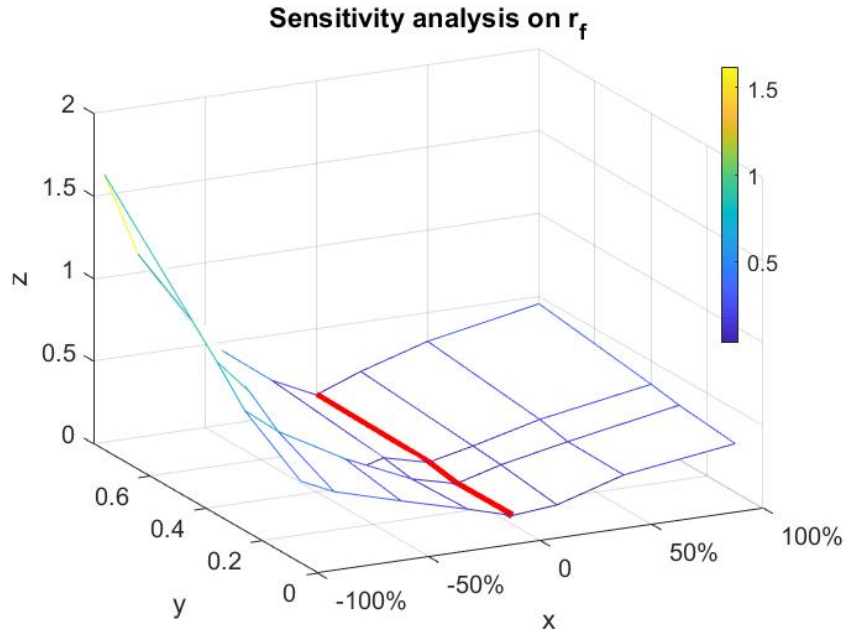
Figure 4.9: Sensitivity analysis of fault resistance
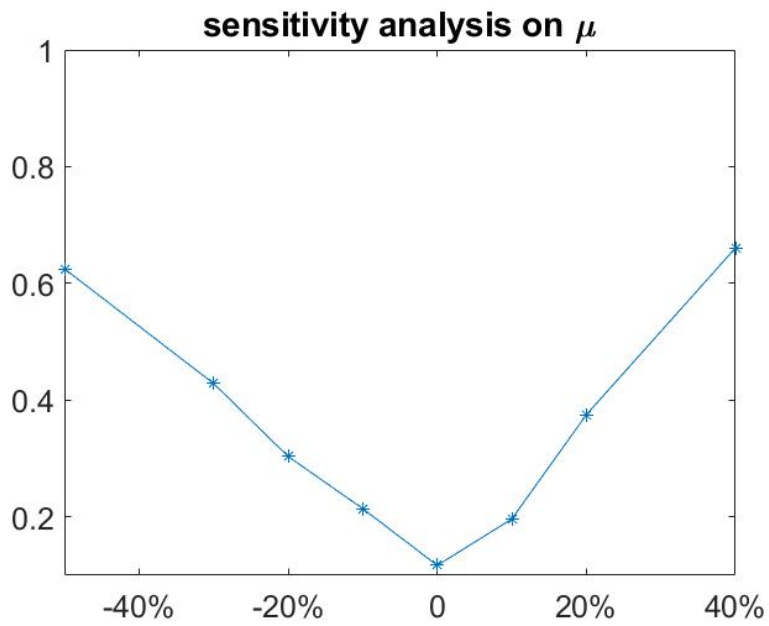
Figure 4.10: Sensitivity analysis of SC ratio with fixed SC ratio
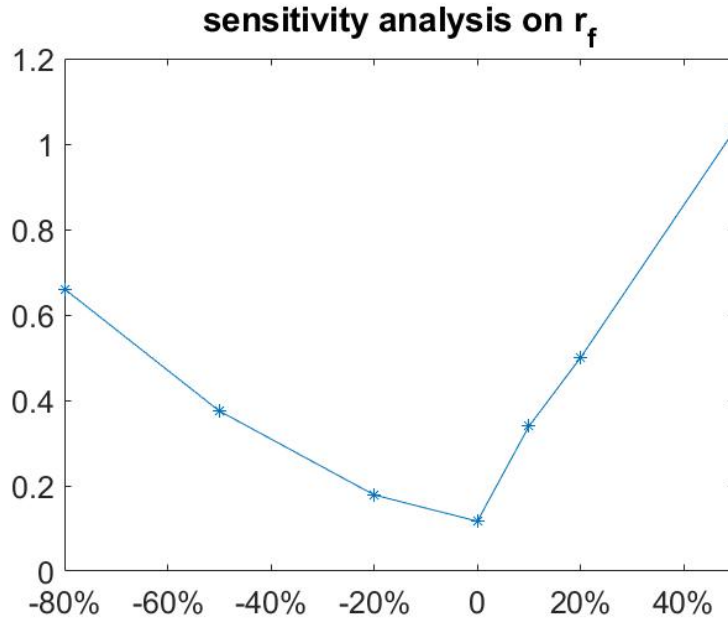
Figure 4.11: Sensitivity analysis of fault resistance with fixed fault resistance

0.4Ω. Based on Fig. 4.10 and Fig. 4.11, same information can be got.

4.4 Experimental Setup

Fig. 4.12 shows the experimental setup. DSP TMS320F28335 development board serves the function of controller. It is worthwhile to note that not just 2 phase currents are measured, but also the fault current is also measured. With fault current measured, fault current measured and calculated can be compared.

Fig. 4.13 shows the hardware setup in experiment.

4.4.1 DSP Development Board

The DSP used in experiment is TMS320F28335. TMS320F2833x devices are part of the family of C2000 microcontrollers, which enables the cost-effective design of intelligent controllers for three phase motors by reducing system components and increasing efficiency. With these devices, it is possible to realize far more precise digital vector control algorithms like the field orientated control (FOC) [22].
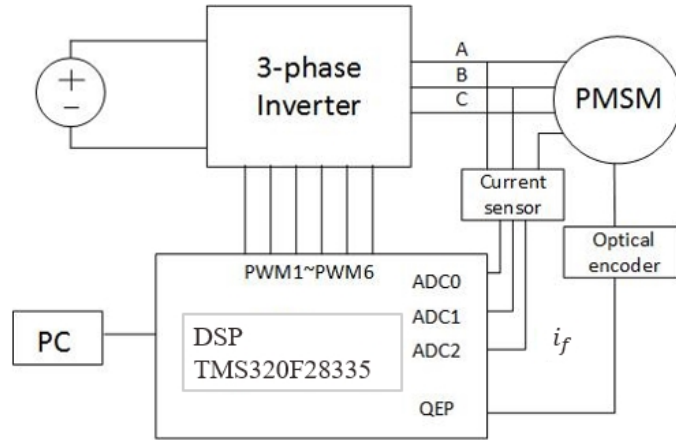
Figure 4.12: Experimental setup
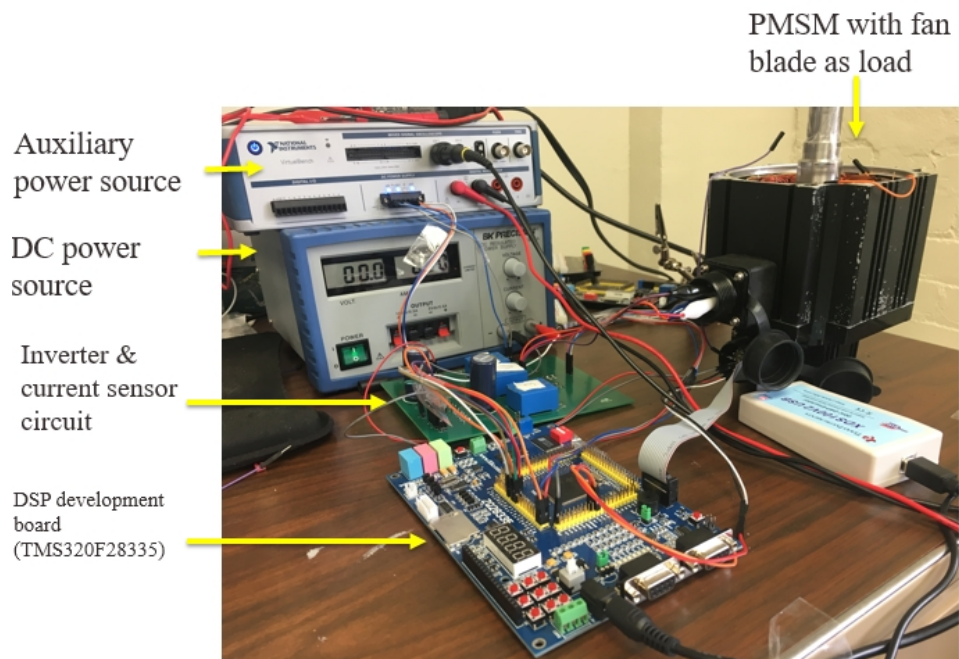
Figure 4.13: Hardware setup in experiment

Appendix. F shows the DSP used in experiment. All pins and components except power supply are displayed.

4.4.2   DSP Program

The program to achieve FOC is developed based on FOC scheme. First, all the module including system clock, PWM, ADC and QEP are initialized as required in the motor drive system. The main program is interrupt-controlled. An interrupt function is used to sample current, calculate speed and determine the gating driver signal. Meanwhile, current in phase A and B are recorded for calculation of output torque.

As for FT control, a variable is set to start FT control. Once FT control works, the additional current component will be calculated and added on original current reference. Then the gating driver signal is generated based on hysteresis control in the interrupt. A minor difference is the fault current also recorded for calculation of output torque.

4.4.3   PCB Design

Appendix. F shows the schematic and layout of PCB designed in the experiment. Its main function includes inverter and current conversion. IRAMS10UP60B is an inverter IC. 3 LA-25-NP are current sensors. The 2 anti-parallel diode BAV99 limit the input pin voltage between 0∼3 V for the protection of DSP chips.

The inverter IC used is IRAMS10UP60B. International Rectifier's IRAMS10UP60B is an Integrated Power Module developed and optimized for electronic motor control in appliance applications such as washing machines and refrigerators. Plug N Drive technology offers an extremely compact, high performance AC motor-driver in a single isolated package for a very simple design. The integration of the bootstrap diodes for the high-side driver section, and the single polarity power supply required to drive the internal circuitry, simplify the utilization of the module and deliver further cost reduction advantages [24]. Its connection is shown in Appendix. F.

The current sensor used is current transducer LA25-NP. It is designed for the electronic measurements of current: DC, AC, pulsed..., with galvanic isolation between the primary circuit and the secondary circuit. The turn ratio selected is 5/1000[25].

4.5 Experimental Results

The left figure in Fig. 4.14 shows the SC point, where the insulation of wire is worn out by sand paper and a wire is soldered. This wire is externally connected with a power resistor to emulate the fault resistance r_f. A hole has to be drilled in the PMSM shell to have the wire externally extended.
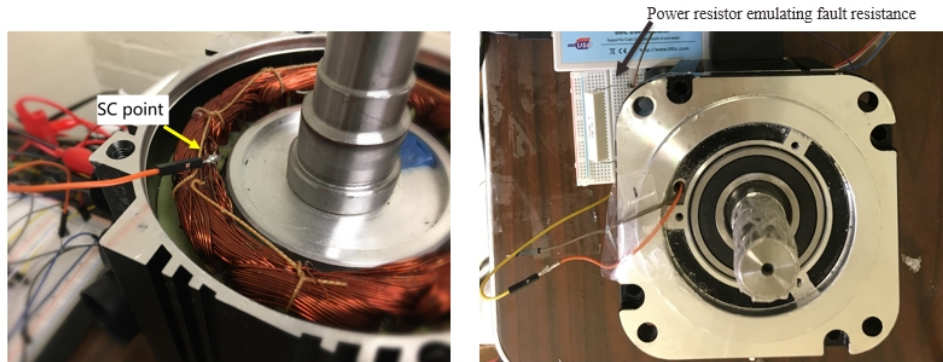
Figure 4.14: Setup of SC fault

Fig. 4.15 shows the comparison of calculated fault current in the controller and filtered measured fault current in the PMSM in FT mode. Fig. 4.16 shows the torque ripple in 3 cases. 68.3 % torque ripple reduction is achieved.
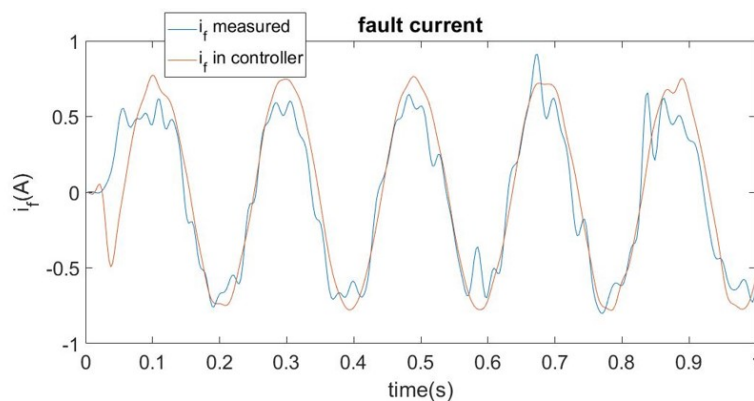
Figure 4.15: Fault current measured and calculated in experiment

30
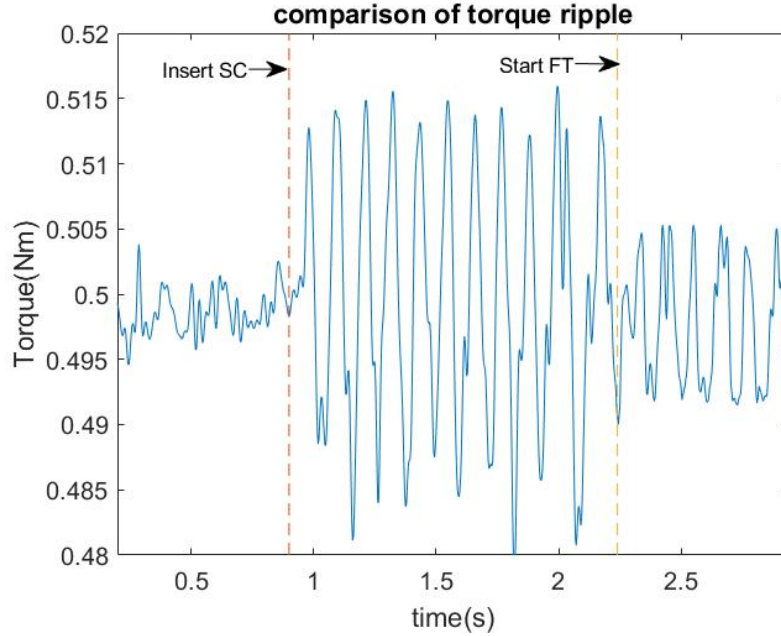
Figure 4.16: Torque in experiment

The torque is not directly measured. Instead, it is calculated with measured current with equation 3.11.

4.6 Sensitivity Analysis and Comparison

Both simulation and experimental results are based on the condition that all PMSM parameters are known. However, as mentioned in simulation, fault parameters in practice are unknown and can only be estimated. Similarly, sensitivity analysis is also performed both in experiments.

Fig. 4.17 shows how estimation accuracy of μ_{sc} affects the torque ripple, while Fig. 4.18 shows how estimation accuracy of r_f affects the torque ripple. The x axis is the estimation error with $\mu_{sc} = 0.145, r_f = 0.4\Omega$. The y axis is is ratio of the torque ripple with FT control to the torque ripple without FT control. The curve from simulation is also plotted for comparison.

Based on above Fig. 4.16 and 4.17, following conclusions can be reached:

1. The better the estimation is, the lower torque ripple will be resulted.

2. If the estimation is so bad that FT control may result in higher torque ripple than no FT control, then proposed FT control should not be used. In other words, sensitivity analysis provides
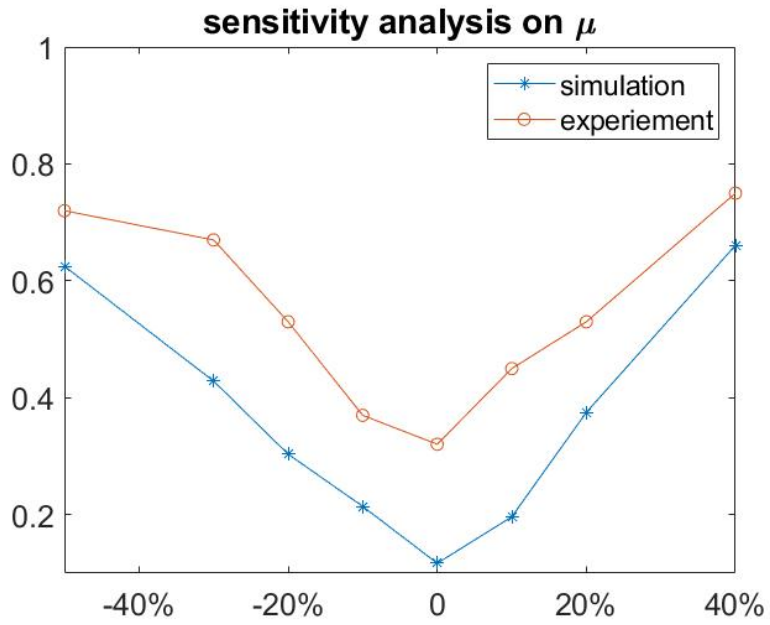
Figure 4.17: Estimated error of SC ratio versus torque ripple
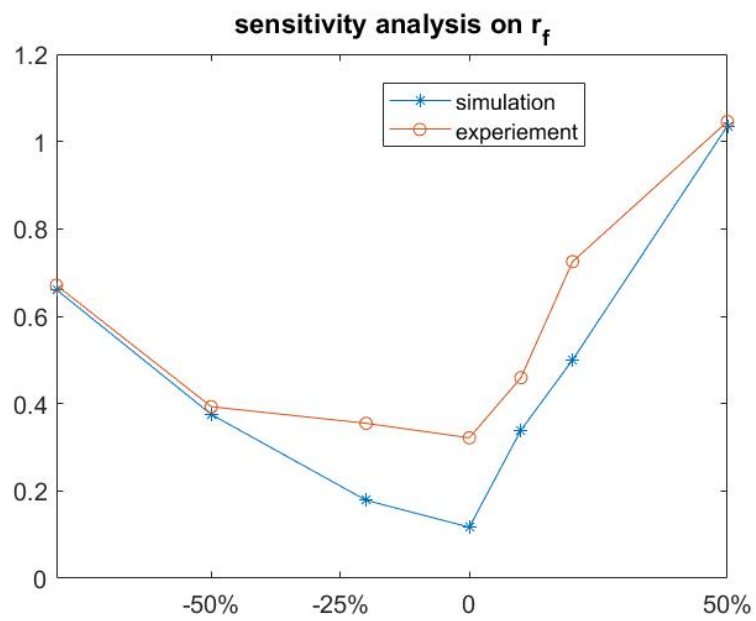
Figure 4.18: Estimated error of fault resistance versus torque ripple

a range of estimation of fault parameters where FT control can reduce the torque ripple.

5.   DIAGNOSIS OF MOTORS WITH SC FAULT[1]

In this chapter, HMM is proposed to estimate fault parameters. The proposed HMM-based diagnosis is initially verified in DC motor, since it has relatively simpler structure and control method than AC motor. After that, it is modified and applied on PMSMs to test its effectiveness.

5.1   Diagnosis of DC Motor

5.1.1   Model of Faulty DC Motor

Fig. 5.1 shows the inter-turn fault inserted on the winding of DC motor. Fig. 5.2 shows the circuit model.
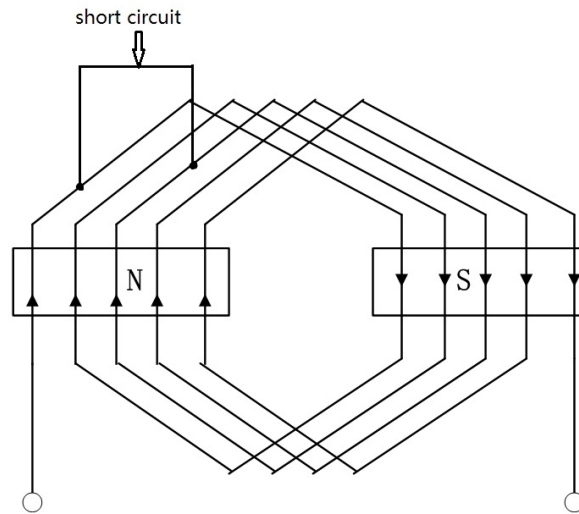
Figure 5.1: The winding diagram with inter-turn SC

SC resistance is an important parameter, which determines the current through the SC point and how serious the fault is. SC ratio refers the ratio between shorted turns and total turns. Even with high SC ratio, the machine can be still in use with high SC resistance. On the contrary, low

---

[1]Section 5.1 reprinted from "On-line diagnosis of inter-turn shortcircuit fault for dc brushed motor" by J.Zhang, W. Zhan, and M. Ehsani, 2018. ISA Transactions, vol. 77, pp. 179- 187, Copyright [2018] by Elsevier.
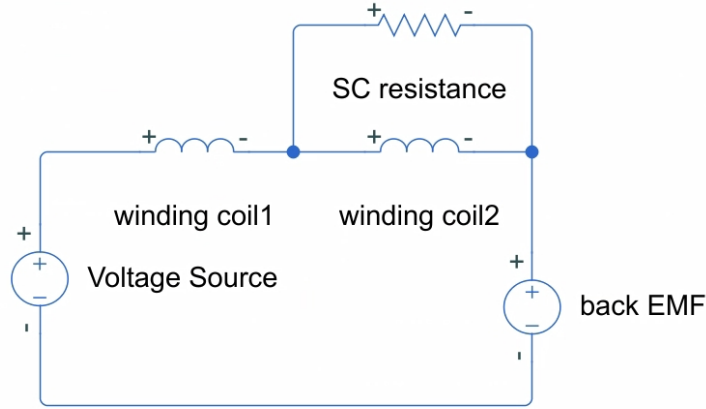
Figure 5.2: Circuit model of DC motor

SC resistance may lead to consideration of repairing due to high temperature and developing fault caused by high fault current. Thereby, SC resistance is as important as SC ratio in evaluation of fault severity.

The objective of diagnosis is to effectively estimate both SC ratio and SC resistance given armature current.

Considering the circuit model, following equations are used to model DC motor

$$
\begin{aligned}
V = E + (1-u)^2 L_a \frac{di_a}{dt} + (1-u)iR_a + u^2 L_a \frac{d(i_a - i_f)}{dt} \\
+ u(i_a - i_f)R_a
\end{aligned}
\tag{5.1}
$$

$$
(1-u) * u L_a i_a + u^2 L_a \frac{d(i_a - i_f)}{dt} + u R_a (i_a - i_f) + uE = i_f R_f
\tag{5.2}
$$

where V represents supply voltage (V), E represents back EMF (V), L_a represents the armature inductance (H), R_a represents the armature resistance (Ω), i_a represents the armature current (A), i_f represents the current through the SC resistance (A), μ represents the SC ratio and R_f represents

35

the SC resistance (Ω). Equation 5.1 is derived based on Kirchhoff Voltage Law applied on the loop excluding the SC resistance. Equation 5.2 is derived based on Kirchhoff Voltage Law applied on the SC loop.

The torque-current equation is modified to reflect the SC effect and shown in 5.3

$$T = K(i_a - ui_f) \tag{5.3}$$

where K is the torque coefficient (Nm/A) and T is the output torque (Nm).

The load torque equation is shown in 5.4

$$T - T_L = J\frac{d\omega}{dt} \tag{5.4}$$

where T_L represents the load torque (Nm), J represents the inertia (kgm^2) and ω represents the speed (rad/sec).

The DC motor drive system to achieve constant speed is modelled in MATLAB/Simulink environment. The closed-loop current and closed-loop speed make up control.

Assumptions are made on how SC ratio affects the machine parameters as shown in equations 5.5 and 5.6.

$$R_{a1} = R_{a0} * (1 - u)\Omega \tag{5.5}$$

$$L_{a1} = L_{a0} * (1 - u)^2 H \tag{5.6}$$

where R_{a0} is the normal armature resistance and L_{a0} the normal armature inductance.

5.1.2 Proposed Method

HMM, a typical pattern recognition method is selected for diagnosis considering its two distinct advantages over model-based diagnosis: 1) it is tolerant to data with moderate deviations; 2) solving complex differential equation can be replaced with simple probability calculation, which improves the efficiency of the algorithm. On the other hand, it is inevitable to require large amount

of data for training.

The following example illustrates the origin of HMM. Suppose there are 3 urns containing a large number of colored balls as shown in Fig. 5.3. An initial urn is chosen, according to some random process. A colored ball is then chosen from this urn as random. The results of the color can be observed in front of the veil. After the color of the ball is observed, the colored ball is replaced in the same urn and a new urn is selected according a random process associated with the current urn. The ball selection process from this new urn is repeated. This experiment generates a finite observation sequence of colored balls. Only the sequence of colored balls can be observed in front of the veil.
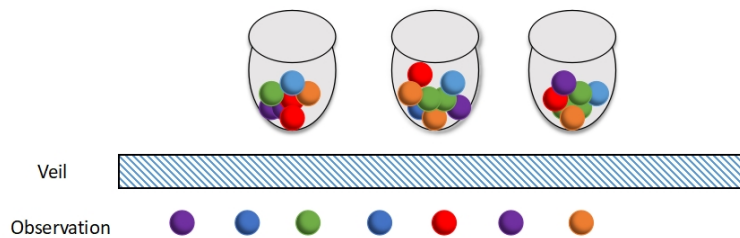
Figure 5.3: The urn-ball problem

The problem of interest is how to know the sequence behind the veil, which is effectively solved by HMM.

This example and the diagnosis share similarities in many aspects. If the value of armature current represents the color of balls, then different values correspond to different colors. Based on colors of balls, it is required to infer the urn sequence. Similarly, based on the value of armature current, the fault or its severity can be also inferred.

Usually, a decision of diagnosis is made by comparing with some thresholds [26]. However, two issues have to be taken into consideration in this process. First, thresholds are difficult to set due to unknown deviations unless an exact model is built to predict the deviation. Besides, data features is inevitably deviated as a result of many comprehensive factors, such as measuring error,

external disturbance. Therefore, it is not always reliable to classify or diagnose given thresholds.

With its learning and statistics characteristics, HMM is a candidate to solve above problems. The initial idea of HMM being used in diagnosis results from the similarities of task between fault diagnostic and speech recognition. Speech recognition is achieved by recording and analyzing the sound waveform, while the fault diagnostic works by measuring and analyzing the observed waveform, such as armature current of DC motor. Moreover, speech recognition requires recognition from vocabulary with a large amount of words, while the fault is classified in one of fewer categories, further making this application relatively simple and feasible. With training by known data features, HMM is expected to capture the significant feature of waveform and thereby classify waveform, that is, the fault diagnosis.

A HMM consists of Markov chains whose states cannot be observed directly. Fig. 5.4 shows a typical HMM containing states connected by transitions. The transition is usually described by a transition probability matrix, while each state is characterized by an observation probability that defines the conditional probability of each observation given certain state. Given the model parameters and the observation sequence it is possible to infer the state sequence and HMM. The observation is a vector data features.

Given the background of raising HMM, three key issues stated in [27] wait to be solved before applied:

(1) The evaluation problem: Given model parameters and data features, the problem is how to compute the probability that data features is produced by one model.

(2) The re-estimation problem: Given data features, figure out how to optimize model parameters.

(3) The decoding problem: Given data features, derive which state sequence is the most probable.

Solution of above problems are researched and provided in [27]. Forward and backward algorithm can compute the probability of the first problem. Baum-Welch re-estimation algorithm and Viterbi algorithm provide solutions for the second problem and the third problem respectively.
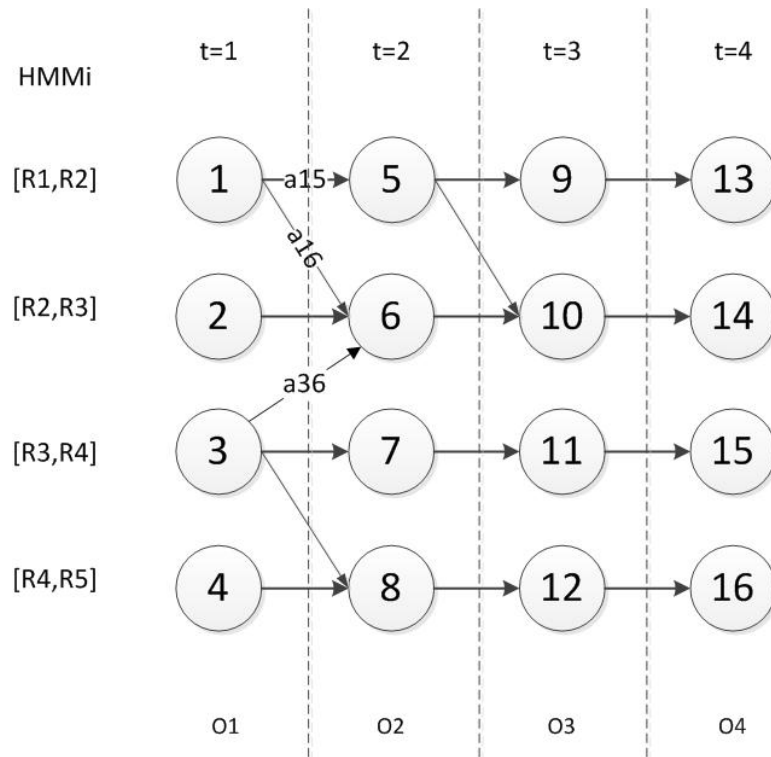
Figure 5.4: HMM for diagnosis (only part of transition shown)

5.1.3 Applications on DC Motor with Inter-turn SC

In this section, the feasibility of applying HMM on inter-turn SC fault diagnosis will be studied.

Multiple HMMs are required and different HMMs can represent different SC ratios. In its simplest form, each HMM can be trained by data with a specific SC ratio and when a new data is provided to the model it returns a log-likelihood of the data being generated from each HMM [28]. In this work, 4 HMMs represent specific SC ratio 0% (no fault), 10%, 15% and 20% respectively. One can certainly select arbitrary values as SC ratio such as 25%, 30% etc. However, if the SC ratio is too small (5%), the false positive will be greatly increased.

5.1.3.1 *Design of HMM*

Design of HMM is a chicken or the egg problem. It requires the information of distribution of data features. However, the design will affect the distribution in turn. Initial HMM is designed and then feasibility is validated over distribution. And the feedback information helps adjust the initial

39

HMM. Part of this process is shown in the subsection of Distribution of Data Features.

To briefly introduce the structure of HMM, the final HMM is given in Fig. 5.4. In each waveform, a period of time series is segmented into few intervals. It is selected to set 4 states per sequence which will be explained in the following subsection. Since SC resistance is a key factor to be estimated, each SC resistance intervals corresponds to a sequence. Each model is trained by data with 4 SC resistance intervals respectively. These values are not fixed and can be adjusted by experience or actual requirements. Therefore, there are 16 states in each model as shown in the Fig. 5.4.

In Fig. 5.4, different row represents different SC resistance intervals. For example, if the fault situation is $R1 < R_f < R2$, the state 1,5,9, and 13 are more likely to be selected to make up the state sequence. And on the other hand, if state 1,5,9, and 13 are selected, it can be inferred that fault resistance is more likely to be between R1 and R2. Transitions between states in different rows are reserved for resistance close to the specified resistance values above.

5.1.3.2   HMM Parameters and Initialization

Key parameters in the HMMs should be reasonably initialized as discussed following.

$\pi = [\pi_i]$, where i $\in$ [1,4], represents the initial state distribution. It is equally initialized in each HMM. One constraint is $\sum_i \pi_i = 1$.

$A = [a_{ij}] \big| a_{ij} = P(s_{t+1} = j | s_t = i)$, represents the state transition probability distribution, where a_{ij} denotes the transition probability from state i to state j. Three constraints are imposed given practical application. First, $\sum_j a_{ij} = 1$. Second, $a_{ij} \neq 0$ only when $7 \geq j - i \geq 4$, considering that transition irreversibly occurs between adjacent segments. Third, no transition should be initialized as 0 unless it is always 0 since the algorithm does not change transitions value with 0. TABLE 5.1 shows the initialization of transition matrix used here.

For example, the number stored in the row index 2 and column index 6 denoted as a_{26} is the transition probability from state 2 to state 6. Since all four non-zero sub-matrix share the same initialization, only one sub-matrix is displayed. The elements initialized as 0 are not shown, such as a_{11}, a_{12}.

Table 5.1: Part of Initialization of transition matrix

Index	5	6	7	8
1	0.9	0.09	0.01	0
2	0.09	0.81	0.09	0.01
3	0.01	0.09	0.81	0.09
4	0	0.01	0.09	0.9

$B = [b_j(o_t)] | b_j(o_t) = P(O_t | S_t = j)$, represents the corresponding output probability of data feature given certain state. To initialize it, data feature and its distribution should be studied.

5.1.3.3 *Distribution of Data Features*

Different from ac motors where frequency domain provides data features, time domain is the main option of data features. As both SC ratio and resistance are concerned, at least two data features are necessarily required. To select data features, attention should be paid on how SC affects the current waveform. Fig. 5.5 shows one PWM period of current waveform from simulation.
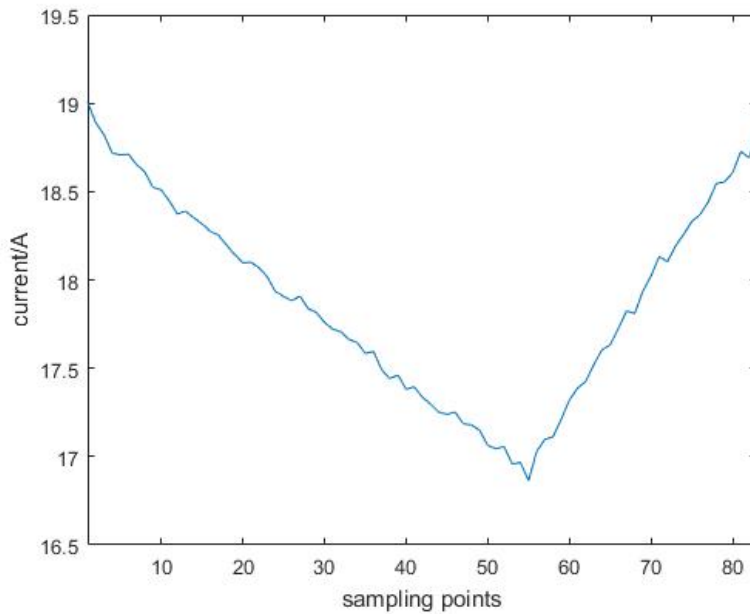
Figure 5.5: Current waveform within one PWM period

Assuming constant SC resistance, the higher the SC ratio is, the less the impedance of changing current and thereby the quicker the current increases and decreases. Slope can be used to assess the changing rate of current and is thereby an option of data features. For convenience, slope used in this paper refers the absolute value of change of current per unit time instead of the changing rate.

Similarly, assuming constant SC ratio, the less the SC resistance is, the higher average current is required to generate constant load torque. Therefore average current is also taken into consideration. Following work will verify whether these two can be used as data features.

Combination with HMM theory, the number of states should be determined. Fewer states leads to low accuracy in recognition, since information of data features is omitted while decreasing states. More states inevitably result in larger amount of calculation and data storage. Considering both aspects, the number of states selected is 4, which has good accuracy and reasonable amount of calculation.

Based on above discussion, the issue arises how to determine 4 states within one PWM period of current. The intuitive way is to averagely segment the current period into 4 states or segments as shown in Fig. 5.6.

However, it is validated in the Fig. 5.7 that the slope of current in the third state largely coincides in the distribution of different SC ratio and thereby is not helpful in recognition of SC ratio. If this state doesn't contain both increasing and decreasing slope, the issue will be solved. Fig. 5.8 shows the improved segment of states. The first 2 states are averagely segmented, so as the last 2 states.

It is required that all features of data under unknown deviations fit the normal distribution considering convenience of calculation. Thereby, Central limit theorem is applied. Average of data features are extracted. When the number of samples averaged being sufficiently large, the average can be approximated by normal distributions. The number of samples selected here is 30.

Distributions of data features in different conditions of state 3 are scattered in the Fig. 5.9. The SC resistance varies from 0.03Ω to 300Ω. 0.03Ω is close to represent complete SC, while 300Ω
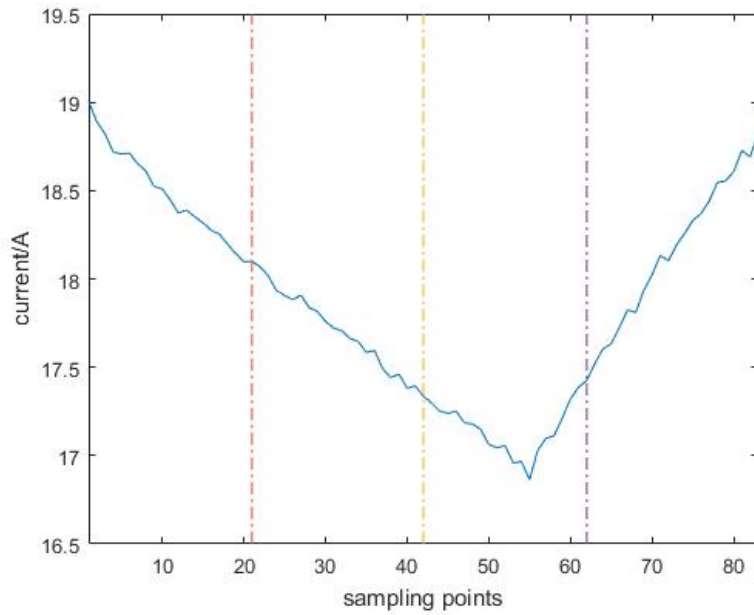
Figure 5.6: Current waveform with average segment
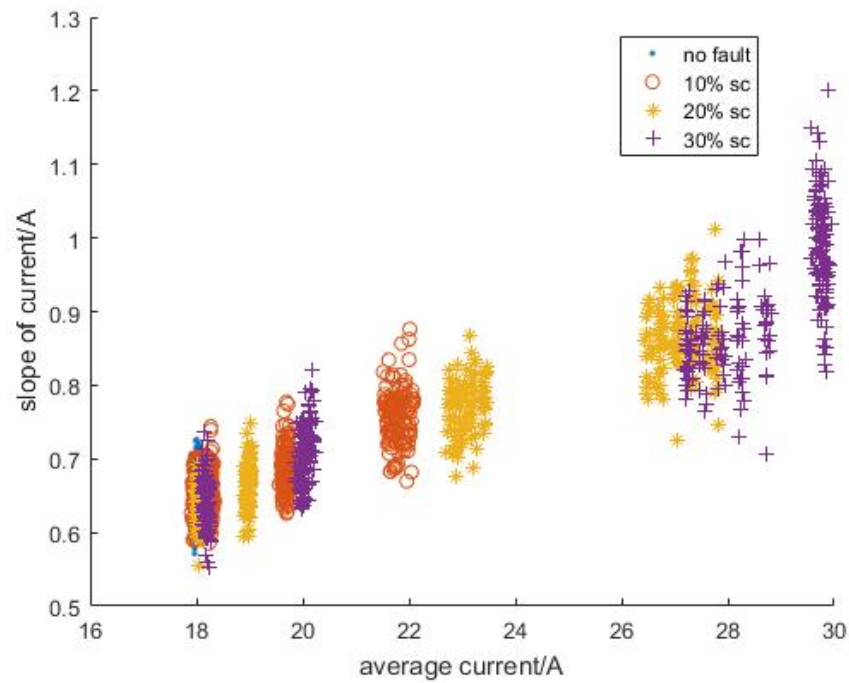
Figure 5.7: Distributions of data feature in state 3
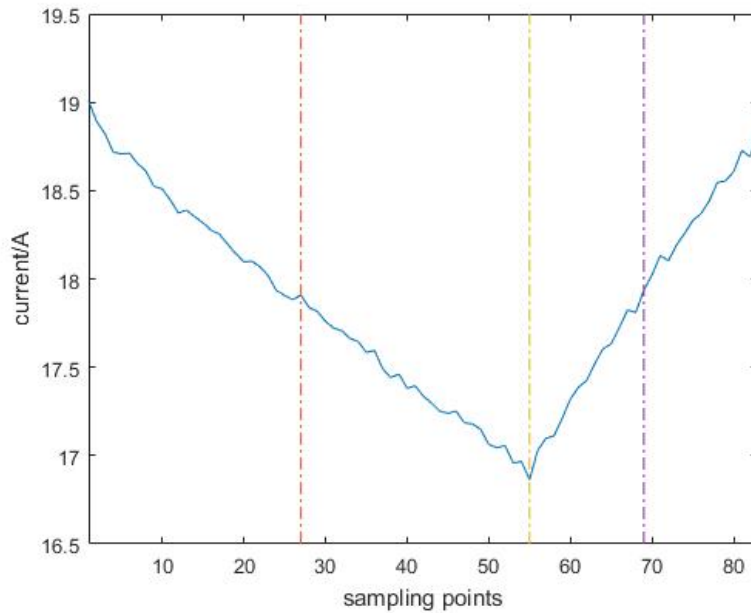
Figure 5.8: Current waveform with modified segment

represents no fault compared with 10Ω armature resistance. It is validated that distributions of other states have the similar pattern.

With observations of these data distributions, it is easy to find that these data distributions with different SC ratio coincide in certain conditions. It is validated that this only happens when the SC resistance is more than 200Ω, in which case it can be classified as no fault. Therefore, set R1, R2, R3, R4, R5 as 0.03, 0.3, 3, 30, 200Ω respectively.

Fig. 5.9 clearly shows that slope works in differing SC ratios. Fig. 5.10 shows how SC resistance affects the average current with 10% SC ratio. It is observed that the less SC resistance is, the more average current is. And for other SC ratio and segments, same rule applies. Since figures are similar, they are not displayed here.

Conclusion is reached that slope and average can be used as data features in estimation of inter-turn SC degree.

Since distributions of average of data feature approach to normal based on Central limit theorem, normal distribution formula is selected for probability calculation. Equation 5.7 is used to
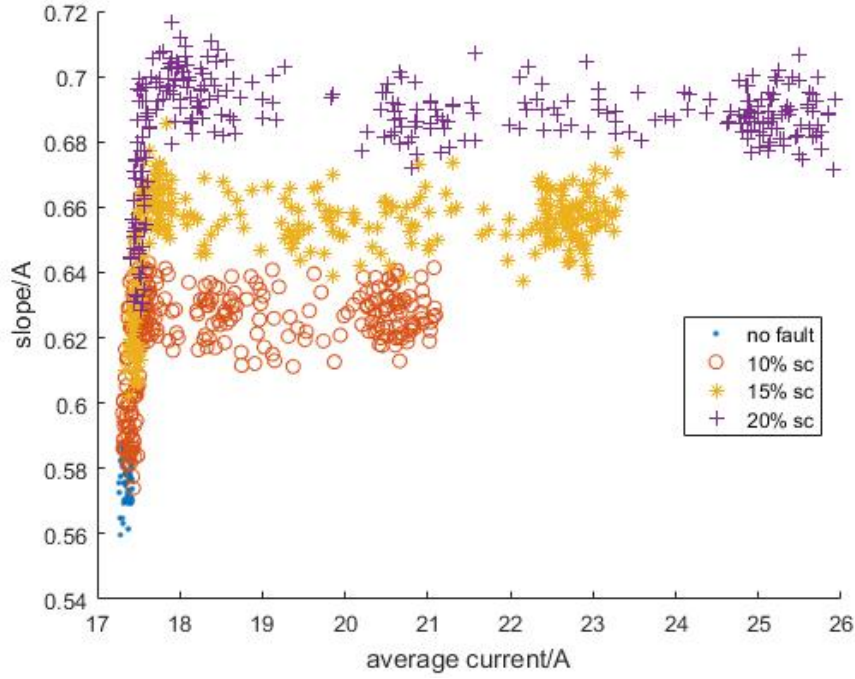
Figure 5.9: Data distributions of segment 3

calculate the output probability density.

$$b_j(o_t) = \frac{1}{\sqrt{(2\pi)^3|B_{cov}(j)|}}exp(-\frac{1}{2}(o_t - B_{exp}(j))^T$$
$$(B_{cov}(j))^{-1}(o_t - B_{exp}(j))) \tag{5.7}$$

where $B_{exp}(j)$ represents the expectation vector of multivariate normal distribution in state j and $B_{cov}(j)$ represents the covariance matrix of multivariate normal distribution in state j. Initialization of output probability matrix is based on few samples of data features.

5.1.3.4   HMM Algorithms

After initialization, there are two necessary steps to follow, re-estimation and recognition. Re-estimation algorithm is executed to optimize the HMM parameters including π, A and B
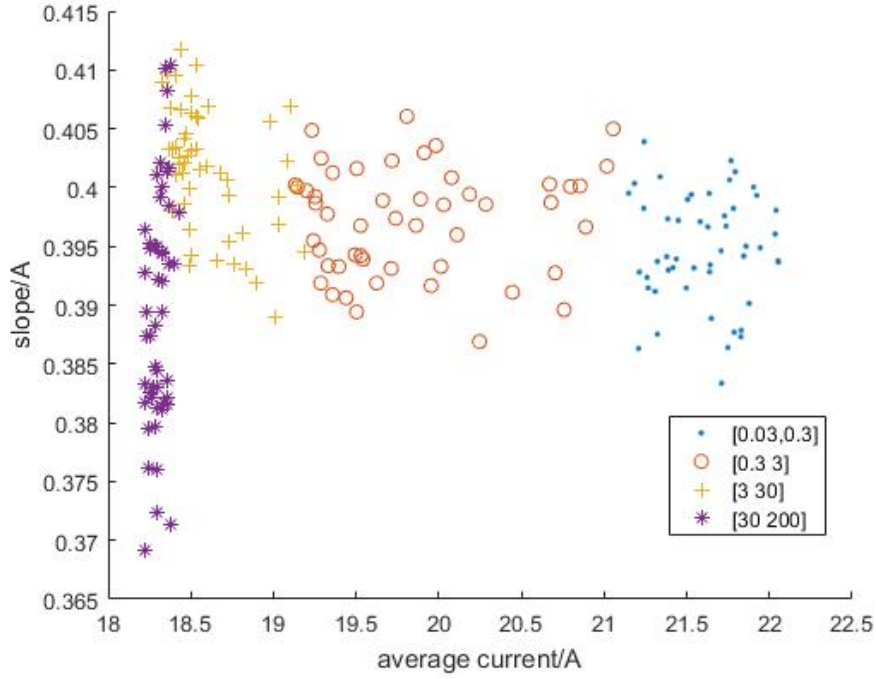
Figure 5.10: Data distributions of segment 1 with 10% SC

matrix, all together denoted as λ. Let $O^M = [O^1, O^2, ..., O^m]$ denotes the set of m data features, the objective of optimization is maximization of

$$logPr(O^M|\lambda) = \sum_{n=1}^{m} logPr(O^n|\lambda) \tag{5.8}$$

It is verified that the parameters of HMM converges with Baum-Welch re-estimation algorithm [27].

Following work is the recognition of model or the estimation of fault severity. The process of recognition is shown schematically in Fig. 5.11. In recognition, the degree of similarity is compared between extracted features to be diagnosed and features used in the training step. The result of comparison between the two features is calculated as likelihood based on forward algorithm. The higher the likelihood is, the more similar the two data features are to each other. The data is categorized with the model with the highest likelihood.

46
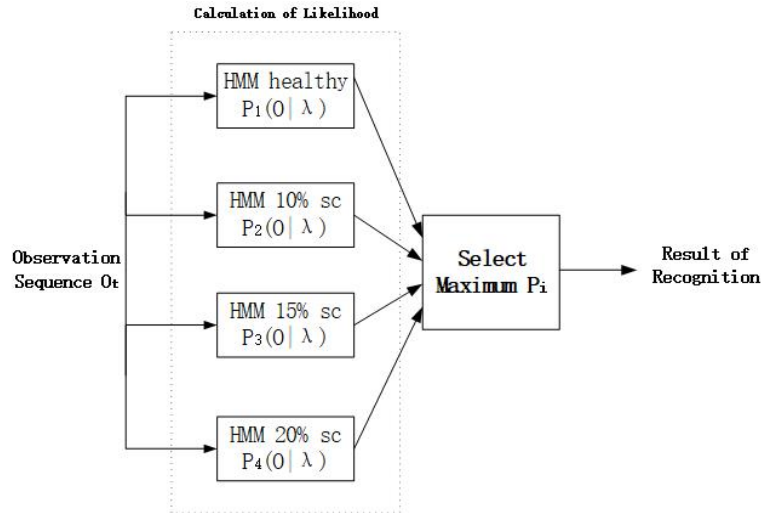
Figure 5.11: Recognition of HMM

5.1.3.5 *Implementation Procedure*

This section concludes necessary steps for implementation.

1) Generate data for training. If the data comes from simulation, the faulty model will be simulated to generate data. To simulate reality, parameters variations and errors should also be added in simulation as already stated. Or the data can come from experiments.

2) Extract data features for training.

3) Initialize HMM parameters.

4) Re-estimate HMM parameters.

Steps 2, 3 and 4 make up the training.

5) Extract data features for validation.

6) Calculate the likelihood and estimate the SC ratio and resistance.

The flow diagram in Fig. 5.12 illustrates above steps.

5.1.4 Simulation Results

With data from the modeling and simulation parts, each HMM is trained by 80 data features and 100 data features are used to validate its accuracy.

The validation result of no fault is 100% in accuracy. Therefore, no false positive will happen.
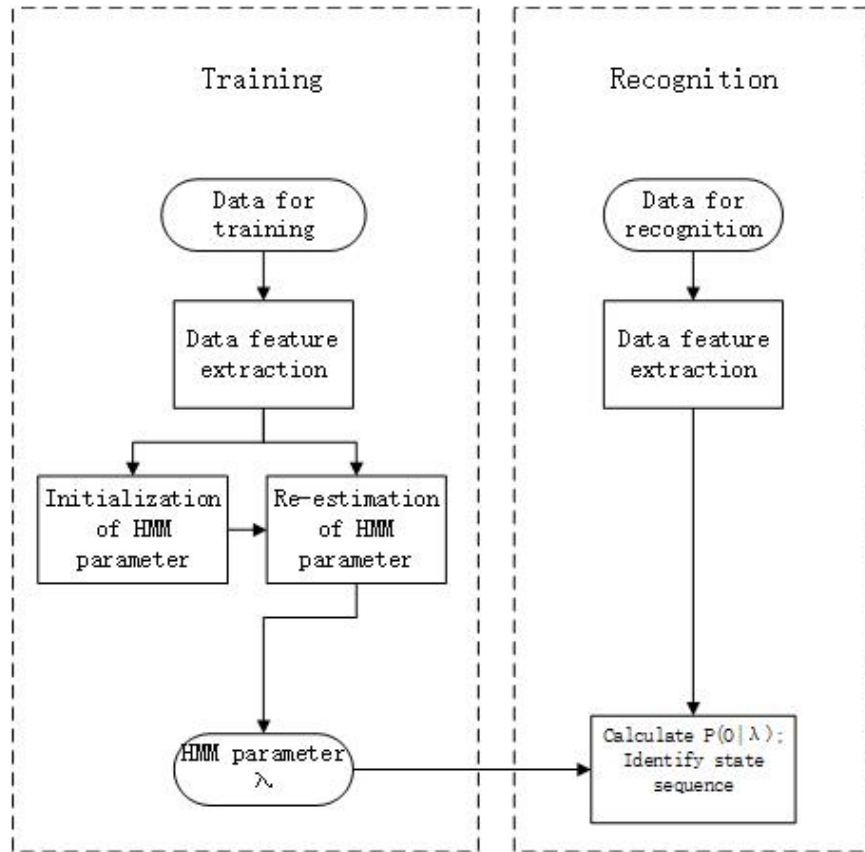
Figure 5.12: Flow diagram

The validation results of different SC ratios and different SC resistances are shown in the Fig. 5.13-Fig. 5.15. It should be noted that the SC resistance can be arbitrarily selected, since SC resistance can be any value. Here it is increased by multiplication of 1.5 instead of linearity to cover a broader range [0.015,168].

It is quite clear that for most SC resistance, the accuracy is 100% or very close to 100%. However, accuracy as low as 60% still exists. Table 5.2 shows the detailed classification of data features with accuracy less than 90%.

As shown in Table 5.2, the left two columns represent the real condition of data used in the validation. Other columns record the classification and its corresponding percentage. Take the first row as an example. The first row represents data features coming from 10% SC ratio and 0.58Ω SC resistance has 82% accuracy, while the other is classified as 10% SC ratio but lower SC resistance.
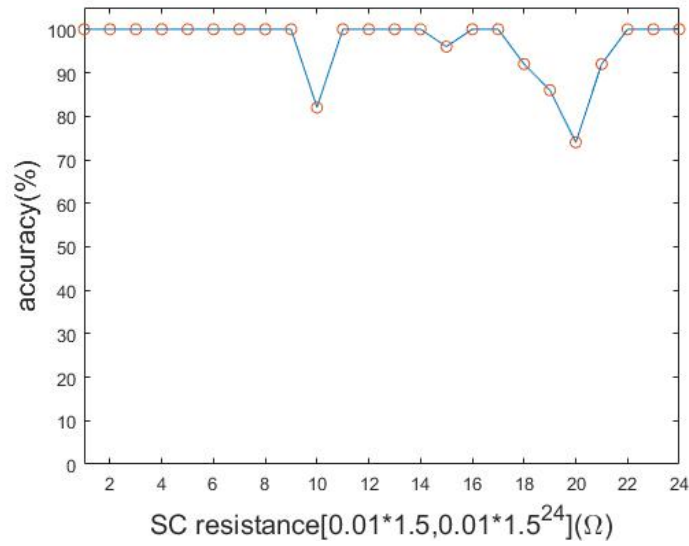
Figure 5.13: Accuracy with 10% SC ratio
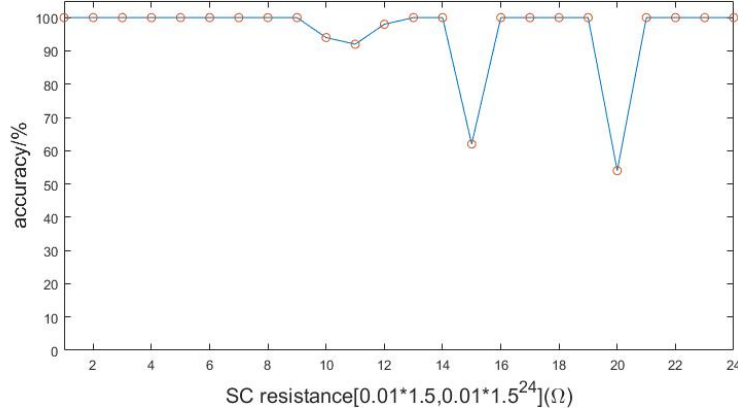
Figure 5.14: Accuracy with 15% SC ratio

Considering this resistance close to 0.3, it does no harm to understanding of the real SC condition. The same explanation can be applied to others.

For now, it is sufficient to say that HMM works under these certain conditions, that is, specific SC ratio and variable SC resistance. However, SC ratio is also continuous and not limited to these specific values in reality. Investigation on other SC ratios such as 12%, 17% needs to be done.

Without modification of the algorithm, data features with some SC ratios is classified as shown

49
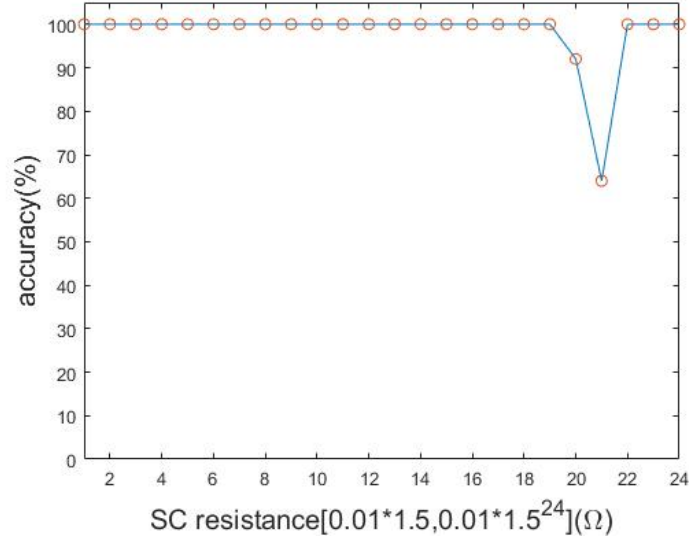
Figure 5.15: Accuracy with 20% SC ratio

Table 5.2: Classification of data with low accuracy

SC ratio	R_f	SC ratio, $[R_{f1},R_{f2}]$, %	SC ratio, $[R_{f1},R_{f2}]$, %
10%	0.58	10%, [0.3,3], 82%	10%, [0.03,0.3], 18%
10%	22.17	10%, [3,30], 84%	15%, [30,200], 16%
10%	33.25	10%, [3,30], 34%	10%, [30,200], 66%
15%	4.38	15%, [0.3,3], 39%	15%, [3,30], 61%
15%	33.25	15%, [3,30], 59%	20%, [30,200], 41%
20%	49.88	20%, [3,30], 34%	20%, [30,200], 66%

in Table 5.3. For data feature with 12% SC ratio, some of them are classified into 10%, while others are classified into 15%. These two exactly contain 12%. Considering the classification percentage, if the result is scattered in two or more classification instead of severely biased on one classification, it should be recognized between two classifications instead of one classification. As a result, an estimated interval of SC ratio is derived instead of a certain SC ratio. As for the SC resistance, it is always correctly estimated. Therefore, it is concluded that the algorithm can effectively estimate the interval of SC ratio and SC resistance.

Two points are proposed as supplements. First, it is worthwhile to note that the diagnosis

Table 5.3: Classification of data features

SC ratio	R_f	SC ratio, $[R_{f1},R_{f2}]$, %	SC ratio, $[R_{f1},R_{f2}]$, %
12%	0.1	10%, [0.03,0.3], 21%	15%, [0.03,0.3], 79%
12%	1	10%, [0.3,3], 28%	15%, [0.3,3], 72%
12%	10	10%, [3,30], 78%	15%, [3,30], 22%
12%	100	10%, [30,200], 5%	15%, [30,200], 95%
17%	0.1	15%, [0.03,0.3], 21%	20%, [0.03,0.3], 79%
17%	1	15%, [0.3,3], 52%	20%, [0.3,3], 48%
17%	10	15%, [3,30], 64%	20%, [3,30], 48%
17%	100	15%, [30,200], 4%	20%, [30,200], 96%

method validated works under a certain and constant reference speed and load torque, with the requirement of training data being generated in the same condition. It has been verified that even above conditions are changed, the diagnosis can still work in new conditions with training data from new conditions.

Besides, the HMM-based algorithm will classify any data features even including data features with other fault, assuming unlimited precision in calculation. To avoid this confusion, the probability given observation, denoted as $Pr(O|\lambda)$ should be made use of by comparing with a threshold. If the probability is lower than the threshold, it is not adequate to claim the classification. Here it is validated in the simulation work that the threshold is set as 1. If it is higher than this threshold, then judge whether the result is obviously biased on one classification. If so, the classification is done. Otherwise, an estimated interval of SC ratio is given.

A relatively simple application of HMM on diagnosis of fault severity is presented and validated. However, HMM is a general solution in evaluation of fault. With proper modelling and training, it is expected to diagnose other faults and evaluate their severity.

The detailed work and result can refer to [29].

5.2 Diagnosis and FT Control of PMSM

After its successful application on DC motor, the HMM-based diagnosis is modified and applied on PMSMs to do the same work.

5.2.1 Modeling of Faulty PMSM

The modeling of faulty PMSM has been presented in detail in Chap.3. However, there is a slight difference on SC effect on inductance. The follow work proceeds with assumption of a single coil in each phase winding. With this assumption, equations 5.9-5.11 are approximately accurate.

$$L_{as1} = (1 - \mu_{sc})^2 L_s \tag{5.9}$$

$$L_{as2} = \mu_{sc}^2 L_s \tag{5.10}$$

$$M_{as1as2} = \mu_{sc}(1 - \mu_{sc})L_s \tag{5.11}$$

Its model was analyzed in [4, 5]. Its simulation model is built in Simulink similar in Chap.3. FOC was implemented in the simulation to control the motor. The parameter values for simulation are listed in Table 5.4.

Table 5.4: Simulation parameters

Source voltage	460 V
Sampling frequency	100 KHz
Field flux coefficients	0.2 Nm/A
Stator resistance	1.4 Ω
Stator self inductance	10 mH
Stator mutual inductance	-3.4 mH
Reference Speed	1000 rpm
Load torque	8 Nm
Load inertial	0.2 Kgm^2

A Gaussian white noise block in Simulink, with mean set to 0 and standard deviation set to 0.01, was added in each current measurement to simulate noise and measuring error. The machine parameters such as winding self inductance and mutual inductance and resistance are allowed to vary randomly according a uniform distribution within $\pm$ 3% error to account for the manufacturing tolerance.

5.2.2 Analysis of Degrading Performance

Performance metrics of electric motors include torque ripple, speed ripple, power loss and harmonics component of phase current. By inserting inter-turn SC in phase A in the Simulink model, the motor performance with different R_f and constant $\mu = 0.2$ were simulated with the result summarized in Table 5.5 as an example. It can be observed that many variables vary monotonically as fault resistance increases. This property will be used when selecting the data feature.

Table 5.5: Degraded performance with $\mu = 0.2$

$R_f(\Omega)$	0.05	0.25	1.25	6.25
T_{ripple}(Nm)	4.8738	2.8911	0.9798	0.4696
P_{loss}(W)	383	442	499	520
I_{q1}(A)	2.7797	1.6605	0.5665	0.2610
I_{d1}(A)	2.7383	1.6761	0.5801	0.1335
I_f(A)	54.7	32.8	10.7	2.5
Y_{a1}(A)	12.991	11.136	9.266	8.585
Y_{a3}(A)	0.0407	0.0204	0.0047	0.0048
Y_{a5}(A)	0.0027	0.0032	0.0017	0.0024
Y_{b1}(A)	10.928	9.940	8.938	8.552
Y_{b3}(A)	0.0432	0.0252	0.0120	0.0116
Y_{b5}(A)	0.0072	0.0069	0.0070	0.0068

I_{q1} represents main component of quadrature current, I_{d1} represents main component of direct current, I_f represents the current through SC connection, Y_{a1} represents the main component of current in phase A, Y_{a3} and Y_{a5} represent the third harmonics and fifth harmonics. Y_{b1}, Y_{b3} and Y_{b5} represent current components in phase B.

Table 5.6 shows the performance with constant $R_f = 0.25\Omega$ and different μ. Similarly, many variables vary monotonically as μ increases.

One can see from these tables that μ and R_f have significant impact on many motor performance. In particular, power loss and torque ripple are severely affected by inter-turn SC faults. Power loss is mainly caused by small parallel fault resistance. Torque ripple is the result of the

Table 5.6: Degraded performance with $R_f = 0.25\Omega$

μ	0%	10%	20%	30%	40%
T_{ripple}(Nm)	0.1454	0.9893	2.8911	5.3784	8.0875
P_{loss}(W)	219	500	442	359	270
I_{q1}(A)	0.0808	0.5603	1.6605	3.1020	4.5735
I_{d1}(A)	0.0003	0.5639	1.6761	3.0709	4.6418
I_f(A)	0.000	21.1	32.8	40.9	46.0
Y_{a1}(A)	8.782	9.246	11.136	13.574	16.100
Y_{a3}(A)	0.0114	0.0054	0.0204	0.0464	0.0760
Y_{a5}(A)	0.0126	0.0024	0.0032	0.0029	0.0030
Y_{b1}(A)	8.780	8.908	9.940	11.294	12.717
Y_{b3}(A)	0.0106	0.0123	0.0252	0.0474	0.0740
Y_{b5}(A)	0.0116	0.0069	0.0069	0.0073	0.0097

asymmetry among three phases.

5.2.3 Analysis of Fault Features

Fault features used in diagnosis directly determine the accuracy of fault diagnosis. Based on literature review, many different types of features can be extracted for diagnosis of inter-turn SC faults. It can be summarized in following types: 1) stator flux[30]; 2) sequence components of the voltage/current[31], [32]; 3) harmonic component of the voltage/current/power[33], [34]; 4) a mixed set of features including current, voltage, torque, flux and other electrical signals of the machines[35].

There are several specific requirements in selecting fault features. First, features should be distinguishable in quantity for different severity degrees. Second, it is desirable that no additional cost is required. Last, the fault features should be insensitive to noise. The second harmonic component in [33] and increased negative sequence component of the voltage references in [32] provide inspirations for the selection of fault features in this paper. As shown in Tables 5.5 and 5.6, I_{q1} and I_{d1} vary as fault severity varies. Fault features for this specific application can be generated

with Park transformation [36] applied on 3-phase current, as shown in equation (5.12).

$$
\begin{bmatrix} i_d \\ i_q \\ i_n \end{bmatrix} = 2/3 \begin{bmatrix} sin\theta & sin(\theta - \frac{2\pi}{3}) & sin(\theta + \frac{2\pi}{3}) \\ cos\theta & cos(\theta - \frac{2\pi}{3}) & cos(\theta + \frac{2\pi}{3}) \\ \frac{1}{\sqrt{2}} & \frac{1}{\sqrt{2}} & \frac{1}{\sqrt{2}} \end{bmatrix} \begin{bmatrix} i_a \\ i_b \\ i_c \end{bmatrix}
\tag{5.12}
$$

where $\theta = \omega t$ and ω is the angular speed of the reference frame.

Assume harmonics are not present in phase current, therefore, phase currents under the balanced condition can be written as following:

$$
i_a = I sin(\omega_e t)
\tag{5.13}
$$

$$
i_b = I sin(\omega_e t - 2\pi/3)
\tag{5.14}
$$

$$
i_c = I sin(\omega_e t + 2\pi/3)
\tag{5.15}
$$

where I is the amplitude of phase current and ω_e is the electrical angular speed.

Substitute equations (5.13), (5.14), (5.15) into equation (5.12) to get

$$
i_q = I cos(\omega t - \omega_e t)
\tag{5.16}
$$

$$
i_d = I sin(\omega t - \omega_e t)
\tag{5.17}
$$

$$
i_n = 0
\tag{5.18}
$$

The d-q component makes up the positive sequence component.

If 3-phase balance is not satisfied, then

$$
i_q = I_{q11} cos(\omega t - \omega_e t) + I_{q12} sin(\omega t - \omega_e t)
$$
$$
+ I_{q21} cos(\omega t + \omega_e t) + I_{q22} sin(\omega t + \omega_e t)
\tag{5.19}
$$

$$i_d = I_{d11}cos(\omega t - \omega_e t) + I_{d12}sin(\omega t - \omega_e t)$$

$$+I_{d21}cos(\omega t + \omega_e t) + I_{d22}sin(\omega t + \omega_e t) \qquad (5.20)$$

where the I_{q11} and I_{q12} represents the positive component for quadrature current, I_{q21} and I_{q22} represents the negative component for quadrature current. The similar denotation applies for I_{d11}, I_{d12}, I_{d21} and I_{d22}.

In the unbalanced situation, i_a, i_b and i_c also contain the third harmonics with neutral line being used. In that case, equations (5.19), (5.20) can be rewritten as equations (5.21), (5.22)

$$i_q = I_{q11}cos(\omega t - \omega_e t) + I_{q12}sin(\omega t - \omega_e t)$$

$$+I_{q21}cos(\omega t + \omega_e t) + I_{q22}sin(\omega t + \omega_e t)$$

$$+I_{q31}cos(\omega t - 3\omega_e t) + I_{q32}sin(\omega t - 3\omega_e t)$$

$$+I_{q41}cos(\omega t + 3\omega_e t) + I_{q42}sin(\omega t + 3\omega_e t) \qquad (5.21)$$

$$i_d = I_{d11}cos(\omega t - \omega_e t) + I_{d12}sin(\omega t - \omega_e t)$$

$$+I_{d21}cos(\omega t + \omega_e t) + I_{d22}sin(\omega t + \omega_e t)$$

$$+I_{d31}cos(\omega t - 3\omega_e t) + I_{d32}sin(\omega t - 3\omega_e t)$$

$$+I_{d41}cos(\omega t + 3\omega_e t) + I_{d42}sin(\omega t + 3\omega_e t) \qquad (5.22)$$

The positive and negative components of the 3rd harmonics can be obtained by replacing ω with $3\omega_e$ in equations (5.21), (5.22). Considering the precision and amplitude, I_{q11}, I_{q21}, I_{q31}, I_{d11}, I_{d21} and I_{d31} are selected as fault features. Other variables are not selected since their numerical values are less sensitive to severity degrees.

By analyzing the main and harmonics component of sequence current, the information of electrical angle is integrated into data features, which is a clear advantage over the direct harmonics component analysis of phase current. These positive and negative components are selected as fault

features for the forthcoming HMM-based diagnosis and their effectiveness are also validated.

5.2.4 Application of HMM-based Diagnosis and Simulation Results

The application of HMM in fault diagnosis for PMSMs are similar to that for dc motors. The structure of HMM models, the recognition process, and the high level flow diagram for training and recognition are virtually identical to those for dc motors [29]. The only difference is the selected data feature, leading to a different HMM structure shown in Fig. 5.16.
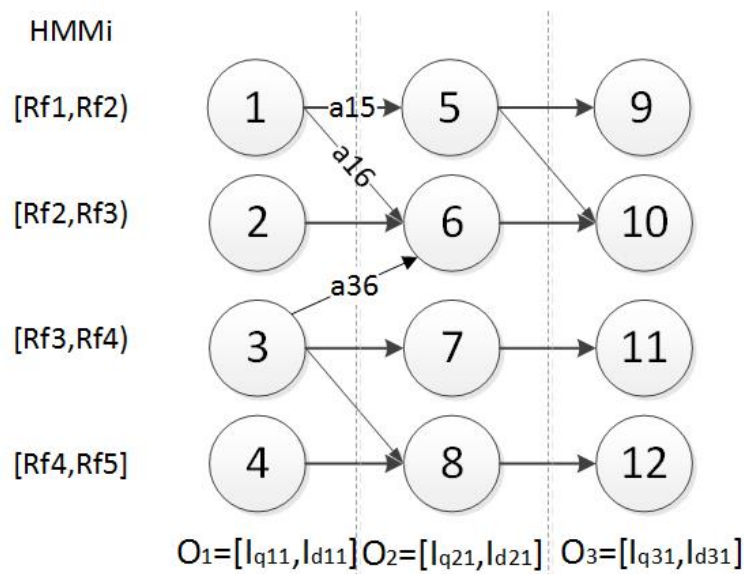
Figure 5.16: HMM for diagnosis (not all transitions are shown)

One hundred simulation data sets were collected for each SC degree value. Fifty of these were used in training, the other fifty were used to validate the accuracy. Table 5.7 shows the accuracy of SC faulty severity estimation based on simulation.

The accuracy for recognizing healthy PMSM is 100% and not shown in the table. For some conditions, the accuracy is not as good as one expected. Most of the errors were from falling into the neighboring categories. For example, $\mu = 18\%$, $R_f = 1\Omega$ is classified as $\mu \in [20\%, 30\%]$, $R_f \in [1.25, 5]$ instead of the correct category of $\mu \in [10\%, 20\%]$, $R_f \in [0.25, 1.25]$.

Table 5.7: Accuracy of faulty severity estimation

R_f	[0.01,0.049]	[0.05,0.249]	[0.25,1.249]	[1.25,5]
μ=5%-10%	87.5%	80.00%	80.00%	82.50%
μ=10%-20%	70.00%	60.00%	70.00%	75.00%
μ=20%-30%	92.5%	75.00%	70.00%	82.50%

5.2.5   Simulation Results of the Proposed FT Control

The FT control in Chapter 3 is still used here. Based on the information provided by the HMM-based diagnosis, estimated intervals are given for μ and R_f instead of values. The intervals cannot be directly substituted into the proposed estimator, which requires values instead of intervals. This issue will be resolved in the next subsection.

First, one would like to verify whether the torque ripple will be reduced under the assumption that the proposed method provides exact information of fault severity. The real inserted fault severity is $R_f = 0.25\Omega$, $\mu = 0.2$. Fig. 5.17 shows the comparison of results with and without FT control. Clearly, significant reduction in torque ripple is achieved roughly 0.05 second after FT control is applied. The steady-state torque ripple in p.u. is equal to 0.018, which is almost equal to the torque ripple value of 0.144 N*m without any fault.
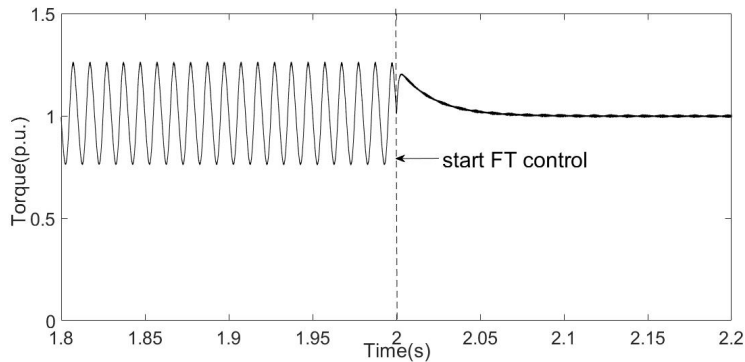

Figure 5.17: Measured torque with and without FT control

5.2.6 Diagnosis-based FT Control

Even though the effectiveness of the proposed method in reducing torque ripple can be easily seen from Fig. 5.17, one must remember that the result is achieved with the assumption that the fault diagnosis provides accurate information about SC ratio μ and SC resistance R_f. In reality, the HMM-based diagnosis algorithm does not provide the accurate information about μ and R_f. Instead, it yields two intervals, one for SC ratio μ and one for SC resistance R_f. The performance of proposed FT control with two intervals for μ and R_f should be verified.

To answer this question, one starts with inspecting the relationship between the current and torque shown in equation (3.11).

From equations (3.3), (3.4), and (3.11) one can conclude that i_a, i_f and i_{afM} should all have the following form.

$$i = A * sin(\theta + \psi) \tag{5.23}$$

where $A = f(\mu, R_f)$ and $\psi = g(\mu, R_f)$. The differences among the three currents are in the different functions of f and g.

After algebraic manipulations of these equations, one can derive an analytic equation for torque as a function of two variables μ and R_f in the steady-state. By varying these two variables one can find out how inaccurate estimation of μ and R_f affect the torque ripple.

Alternatively, one can simply use the Simulink model to get the torque ripple values for different values of μ and R_f. For example, one can use the model to evaluate the real fault severity $\mu = 24\%$ and $R_f = 0.2\Omega$ by replacing μ and R_f with $\mu + \Delta\mu$ and $R_f + \Delta R_f$ in the controller. $\Delta\mu$ is set from -0.05 to 0.05 with an incremental of 0.005. ΔR_f is set from -0.18 to 0.18 with an incremental of 0.03. Fig. 5.18 shows how varying fault severity in the controller affects the torque ripple. It can be seen that there are multiple μ and R_f estimation values that are not necessarily close to the true values but may meet the requirement of torque ripple being below certain threshold. Fig. 5.19 shows these values with torque ripple below 0.2 N*m, which is equal to 2.5% of the

rated load torque.

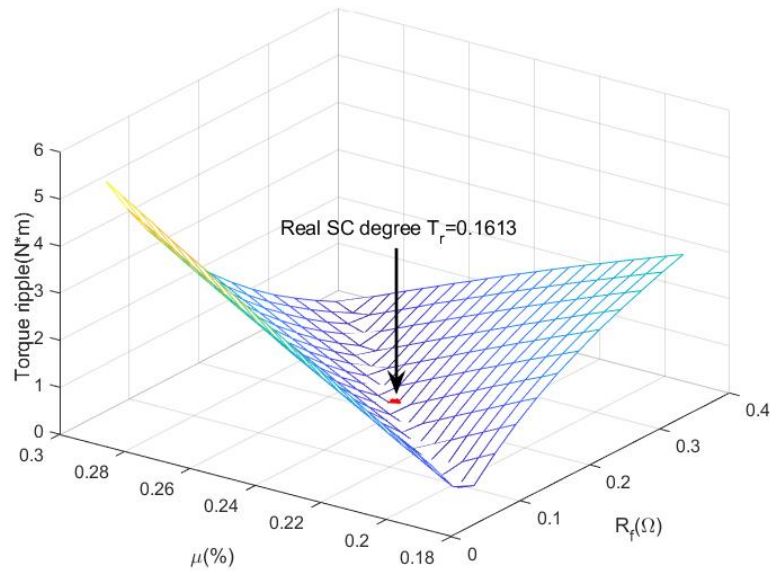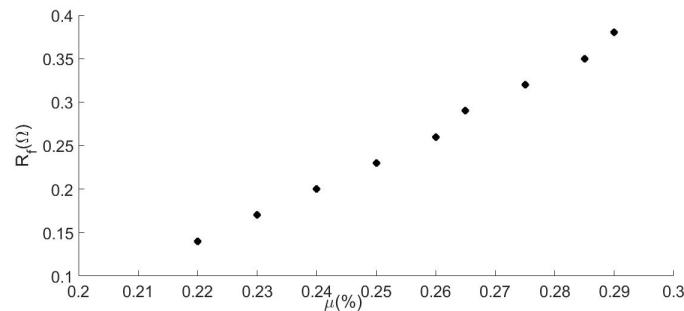Figure 5.18: Torque ripple measured in simulation as a function of μ and R_f

Figure 5.19: Points of fault severity with torque ripple lower than 0.2 N*m

Using Fig. 5.18 or 5.19, one can convert estimation intervals from diagnosis to a single pair of values for SC ratio and SC resistance such that the torque ripple is below a threshold. Two situations are presented to validate the effectiveness of this conversion process.

In the first situation, the diagnosis correctly classifies the fault severity. Take the real fault severity $\mu = 24\%$ and $R_f = 0.2\Omega$ as an example again. It is correctly categorized into $\mu \in [20\%, 30\%], R_f \in [0.05, 0.25]$. Specially, the fault severity $\mu = 20\%$ and $R_f = 0.25\Omega$ falls on the boundary point of the correct estimated interval.

In the second situation, the diagnosis incorrectly classify the fault severity. For example, $\mu = 18\%$ and $R_f = 1\Omega$ is incorrectly categorized into $\mu \in [20\%, 30\%], R_f \in [1.25, 5]$. It should be noted that this type of mistake is inevitable, since the real fault severity is close to the estimated interval as shown in Fig. 5.20.
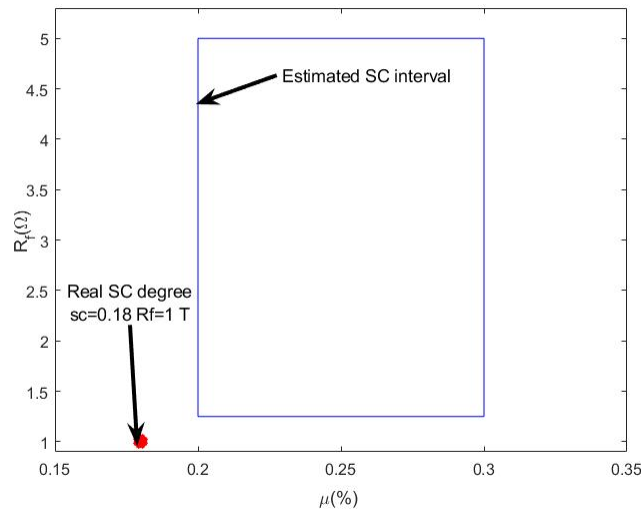
Figure 5.20: Example: incorrectly classified fault severity

In real-world applications, it is not known whether diagnosis is correct or the real fault severity falls on the corner point or not. Therefore, an algorithm is needed to search for the real fault severity or at least the nearby points based on estimated points as shown in Fig. 5.19. A simple bisection search algorithm is applied here. Following steps show how the search algorithm is applied with the first situation $\mu = 24\%$ and $R_f = 0.2\Omega$ as an example. Fig. 5.21 to Fig. 5.24 display each step in the $\mu - R_f$ plane.

Step 1: Four boundary points and the central point are substituted into the estimator for trial, as shown in Fig. 5.21. Stop if one of the points meets the torque ripple requirement. Otherwise continue to next step.
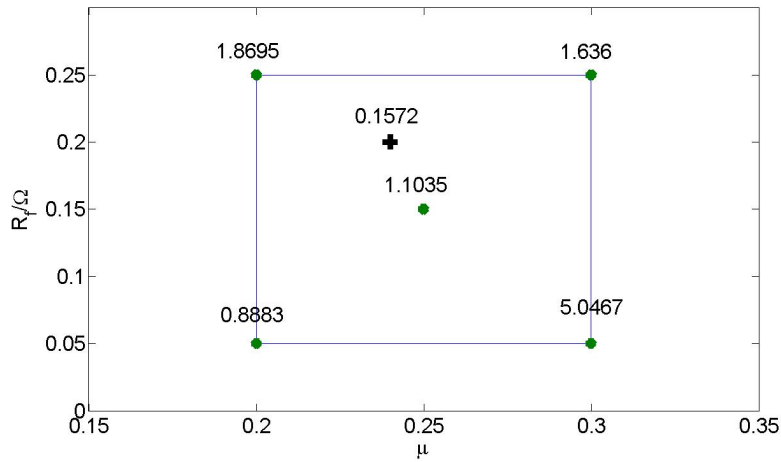

Figure 5.21: Torque ripple with estimated SC parameters: illustration of step 1

Step 2: Try additional points by bisecting the four boundary points, as shown in Fig. 5.22. Stop if one of the points meets the torque ripple requirement. Otherwise continue to next step.
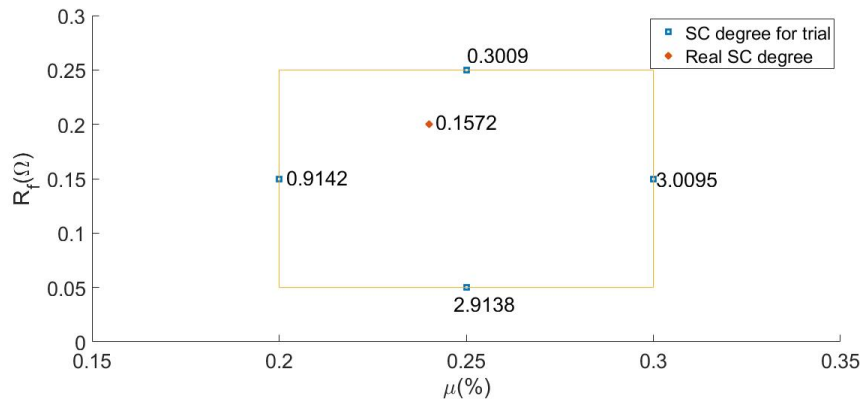
Figure 5.22: Torque ripple with estimated SC parameters: illustration of step 2

step 3: Search among all points already substituted for four points with smallest torque ripple. Get new five points by bisecting these four points and calculating the central point from these four points, as shown in Fig. 5.23. Stop if one of the points meets the torque ripple requirement. Otherwise go ahead to step 4.

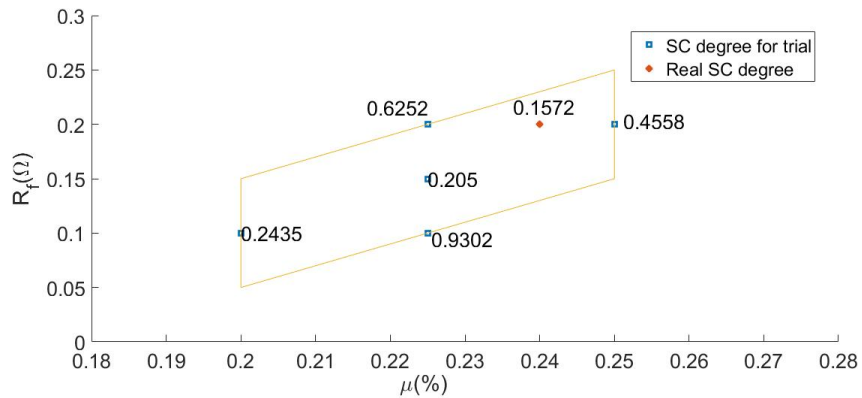Figure 5.23: Torque ripple with estimated SC parameters: illustration of step 3

step 4: Repeat step 3 until a point with torque ripple less than the required value is found, as shown in Fig. 5.24.
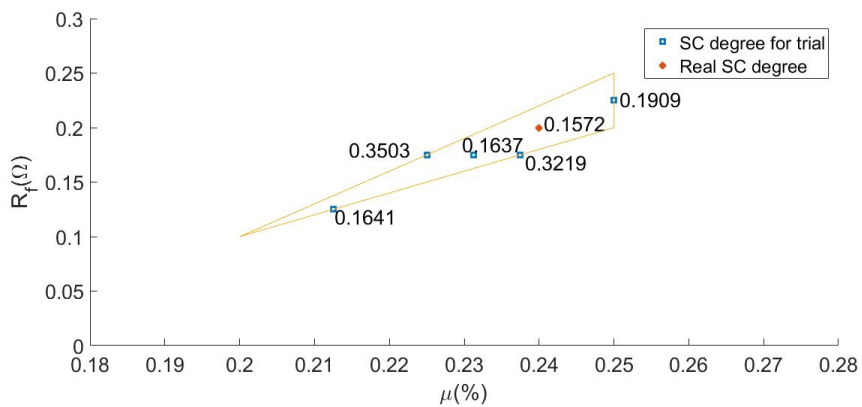

Figure 5.24: Torque ripple with estimated SC parameters: illustration of step 4

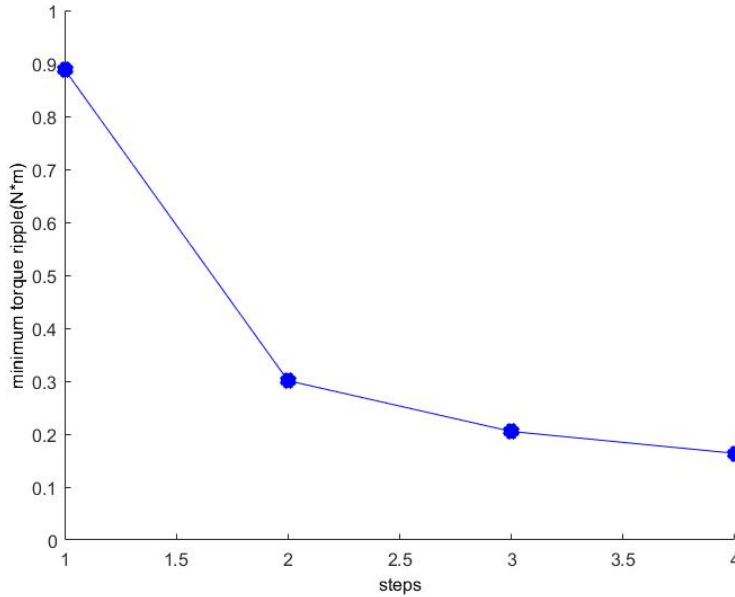The minimum torque ripples in each steps are plotted in Fig. 5.25.

Figure 5.25: Minimum torque ripples versus steps

Simulation results show that the bisection search can effectively find the low torque ripple point. In this example, the torque ripple is found to be reduced to 0.0375 in p.u. compared with no fault torque ripple 0.02 in p.u. within two steps. Continuous search when step 3 is repeated two times, the minimum torque ripple can be reached. After that there is no further reduction the torque ripple. In real-world applications, one may not want to to search for the minimum torque ripple point since the process of trail and error is repeated 19 times in this particular example to gain reduction of torque ripple 0.0175 in p.u.. Depending on the time required for each search step, one may decide to stop searching after certain number of steps. Either an acceptable torque ripple level is achieved or one may conclude that it is impossible to reach the required torque ripple level.

In the second situation, the real fault severity is incorrectly classified. The real fault severity is usually close to a neighboring category. For example, $\mu = 18\%$ and $R_f = 1\Omega$ is incorrectly categorized into $\mu \in [20\%, 30\%], R_f \in [1.25, 5]$. Same bisecting search algorithm can be applied.

It was found that the fault severity $\mu = 20\%$ and $R_f = 1.25\Omega$, resulted in the minimum torque ripple. The reason is that this fault severity is close to the real fault severity. It required 5 trials, as shown in Fig. 5.26. Other incorrectly classified values for fault severity were simulated and the results were similarly acceptable. In summary, the absolute precision of SC fault severity is not necessary for FT control.
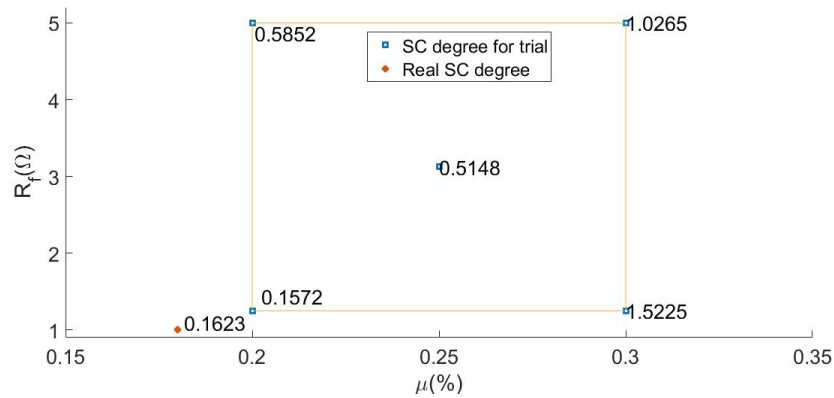

Figure 5.26: Torque ripple with FT control and different estimated R_f and μ

5.2.7 Discussion on Parameter Design of HMM-based Diagnosis

An important issue in HMM-based diagnosis is the selection of the intervals of μ and R_f. The following three factors are considered.

First, one should consider the parameters of PMSM when defining the intervals for R_f. The fault resistance under consideration should not be much larger than the stator resistance of the PMSM. Otherwise, the impact of SC fault on PMSM is negligible and there is no need to identify this faulty situation.

Second, the selection of the intervals of μ and R_f largely dependents on the requirements of the user. The larger the intervals of μ and R_f cover, the more accurate the diagnosis is. On the other hand, if the interval is too large, identification of fault severity will be of less value to the user. In the extreme case where the intervals are so large that only two categories exist, healthy and

faulty. In this case, identification of fault severity degenerates to fault detection. In this sense, the results in this paper can be viewed as a natural generalization of fault detection. The design needs to strike a balance between interval length and accuracy.

Last, FT control plays an important role in the design. In principle, the FT control works even without the HMM-based diagnosis. It just requires more steps in searching for the acceptable torque ripple. HMM-based diagnosis can greatly reduce the searching time. The smaller the intervals are, the more precisely the search area is located; however, it also means more chance for incorrectly categorizing the fault severity. On the other hand, the larger the intervals are, the more time it takes to search. The parameters of HMM-based diagnosis are designed to strike a balance between time and confidence level to reduce torque ripple. The parameters of HMM-based diagnosis are designed to reach the balance of time (maximum 9 times search recommended) and confidence (at least 60% accuracy) to reduce torque ripple less than 0.0375 in p.u..

6. CONCLUSION AND FUTURE WORK

In this work, HMM is proposed to diagnose fault degree of PMSM with inter-turn SC fault. And the original control is reconfigured as FT control, which, on the one hand, decreases the torque ripple, on the other hand, makes use of the faulty phase to maximally retain torque capability.

However, this should not be an end to its application and strength. For FT control, following future work waits to be done:

1.The proposed FT control can be modified and applied on other types of motors.

2. Since the torque ripple in experiment is much higher than simulation, it is expected to build more accurate model to further decrease torque ripple.

3. Or on the contrary, using adaptive control to reduce its dependence on accuracy of modeling and estimation of parameters.

As for diagnosis, following work can be explored:

1. The estimation of fault parameters can be modified and applied on others type of motors.

2. Other types of model-based and statistics-based methods can be studied and applied on identification of fault degree.

REFERENCES

[1] J. G. Cintron-Rivera, S. N. Foste, and E. G. Strangas, "Mitigation of turn-to-turn faults in fault tolerant permanent magnet synchronous motors," *IEEE Transactions on Energy Conversion*, vol. 30, pp. 465–475, June 2015.

[2] B. Gu, "Study of ipmsm interturn faults part i: Development and analysis of models with series and parallel winding connections," *IEEE Transactions on Power Electronics*, vol. 31, pp. 5931–5943, Aug 2016.

[3] I. Jeong, B. J. Hyon, and K. Nam, "Dynamic modeling and control for spmsms with internal turn short fault," *IEEE Transactions on Power Electronics*, vol. 28, pp. 3495–3508, July 2013.

[4] B. Vaseghi, B. Nahid-mobarakh, N. Takorabet, and F. Meibody-Tabar, "Inductance identification and study of pm motor with winding turn short circuit fault," *IEEE Transactions on Magnetics*, vol. 47, pp. 978–981, May 2011.

[5] L. Romeral, J. C. Urresty, J. R. R. Ruiz, and A. G. Espinosa, "Modeling of surface-mounted permanent magnet synchronous motors with stator winding interturn faults," *IEEE Transactions on Industrial Electronics*, vol. 58, pp. 1576–1585, May 2011.

[6] B. Vaseghi, B. Nahid-Mobarakeh, N. Takorabet, and F. Meibody-Tabar, "Experimentally validated dynamic fault model for pmsm with stator winding inter-turn fault," in *2008 IEEE Industry Applications Society Annual Meeting*, pp. 1–5, Oct 2008.

[7] O. Moseler and R. Isermann, "Application of model-based fault detection to a brushless dc motor," *IEEE Transactions on Industrial Electronics*, vol. 47, pp. 1015–1020, Oct 2000.

[8] C. Zhang, F. Wang, Z. Wang, and J. Yang, "Analysis of stator winding inter-turn short circuit fault of pmsm for electric vehicle based on finite element simulation," in *Transportation Electrification Asia-Pacific (ITEC Asia-Pacific), 2014 IEEE Conference and Expo*, pp. 1–6, Aug 2014.

[9] J. Rosero, A. G. Espinosa, J. Cusido, J. A. Ortega, and L. Romeral, "Simulation and fault detection of short circuit winding in a permanent magnet synchronous machine (pmsm) by means of fourier and wavelet transform," in *Instrumentation and Measurement Technology Conference Proceedings, 2008. IMTC 2008. IEEE*, pp. 411–416, May 2008.

[10] S. T. Lee, K. T. Kim, and J. Hur, "Diagnosis technique for stator winding inter-turn fault in bldc motor using detection coil," in *2015 9th International Conference on Power Electronics and ECCE Asia (ICPE-ECCE Asia)*, pp. 2925–2931, June 2015.

[11] S. M. A. Cruz and A. J. M. Cardoso, "Stator winding fault diagnosis in three-phase synchronous and asynchronous motors, by the extended park's vector approach," *IEEE Transactions on Industry Applications*, vol. 37, pp. 1227–1233, Sep 2001.

[12] B. Sen and J. Wang, "Stator interturn fault detection in permanent-magnet machines using pwm ripple current measurement," *IEEE Transactions on Industrial Electronics*, vol. 63, pp. 3148–3157, May 2016.

[13] T. Boileau, N. Leboeuf, B. Nahid-Mobarakeh, and F. Meibody-Tabar, "Synchronous demodulation of control voltages for stator interturn fault detection in pmsm," *IEEE Transactions on Power Electronics*, vol. 28, pp. 5647–5654, Dec 2013.

[14] H. Jeong, S. Moon, and S. W. Kim, "An early stage interturn fault diagnosis of pmsms by using negative-sequence components," *IEEE Transactions on Industrial Electronics*, vol. 64, pp. 5701–5708, July 2017.

[15] H. Nakamura, Y. Yamamoto, and Y. Mizuno, "Diagnosis of short circuit fault of induction motor based on hidden markov model," in *Electrical Insulation and Dielectric Phenomena, 2007. CEIDP 2007. Annual Report - Conference on*, pp. 61–64, Oct 2007.

[16] Y. Fan, C. Li, W. Zhu, X. Zhang, L. Zhang, and M. Cheng, "Stator winding interturn short-circuit faults severity detection controlled by ow-svpwm without cmv of a five-phase ftfscw-ipm," *IEEE Transactions on Industry Applications*, vol. 53, pp. 194–202, Jan 2017.

[17] B. G. Gu, "Study of ipmsm interturn faults part ii: Online fault parameter estimation," *IEEE Transactions on Power Electronics*, vol. 31, pp. 7214–7223, Oct 2016.

[18] B. A. Welchko, T. A. Lipo, T. M. Jahns, and S. E. Schulz, "Fault tolerant three-phase ac motor drive topologies: a comparison of features, cost, and limitations," *IEEE Transactions on Power Electronics*, vol. 19, pp. 1108–1116, July 2004.

[19] T.-H. Liu, J.-R. Fu, and T. A. Lipo, "A strategy for improving reliability of field-oriented controlled induction motor drives," *IEEE Transactions on Industry Applications*, vol. 29, pp. 910–918, Sep 1993.

[20] O. Wallmark, L. Harnefors, and O. Carlson, "Control algorithms for a fault-tolerant pmsm drive," *IEEE Transactions on Industrial Electronics*, vol. 54, pp. 1973–1980, Aug 2007.

[21] C. J. Gajanayake, B. Bhangu, S. Nadarajan, and G. Jayasinghe, "Fault tolerant control method to improve the torque and speed response in pmsm drive with winding faults," in *Power Electronics and Drive Systems (PEDS), 2011 IEEE Ninth International Conference on*, pp. 956–961, Dec 2011.

[22] Texas Instruments, *Sensorless Field Oriented Control of 3-Phase Permanent Magnet Synchronous Motors Using TMS320F2833x*.

[23] J. G. Haitham Abu-Rub, Atif Iqbal, *High Performance Control of AC Drives*. John Wiley, 2012.

[24] International Rectifier, *IRAMS10UP60B Series 10A, 600V with Internal Shunt Resistor*.

[25] LEM, *Current transducer LA25-NP*.

[26] V. Venkatasubramanian, R. Rengaswamy, K. Yin, and S. N. Kavuri, "A review of process fault detection and diagnosis: Part i: Quantitative model-based methods," *Computers & Chemical Engineering*, vol. 27, no. 3, pp. 293 – 311, 2003.

[27] X. D. Huang, *Hidden Markov models for speech recognition*. Edinburgh : Edinburgh University Press, 1990.

[28] O. Geramifard, J. Xu, and W. Chen, "An hmm-based semi-nonparametric approach for fault diagnostics in rotary electric motors," in *Industrial Electronics (ISIE), 2012 IEEE International Symposium on*, pp. 1218–1223, May 2012.

[29] J. Zhang, W. Zhan, and M. Ehsani, "On-line fault diagnosis of electric machine based on the hidden markov model," in *2016 IEEE Transportation Electrification Conference and Expo (ITEC)*, pp. 1–7, June 2016.

[30] J. Penman, H. G. Sedding, B. A. Lloyd, and W. T. Fink, "Detection and location of inter-turn short circuits in the stator windings of operating motors," *IEEE Transactions on Energy Conversion*, vol. 9, pp. 652–658, Dec 1994.

[31] Y. Lee and T. G. Habetler, "An on-line stator turn fault detection method for interior pm synchronous motor drives," in *APEC 07 - Twenty-Second Annual IEEE Applied Power Electronics Conference and Exposition*, pp. 825–831, Feb 2007.

[32] T. Habetler and Y. Lee, "Current-based condition monitoring and fault tolerant operation for electric machines in automotive applications," in *Electrical Machines and Systems, 2007. ICEMS. International Conference on*, pp. 2011–2016, Oct 2007.

[33] T. Boileau, N. Leboeuf, B. Nahid-Mobarakeh, and F. Meibody-Tabar, "Stator winding inter-turn fault detection using control voltages demodulation," in *2012 IEEE Transportation Electrification Conference and Expo (ITEC)*, pp. 1–6, June 2012.

[34] T. Boileau, B. Nahid-Mobarakeh, and F. Meibody-Tabar, "Back-emf based detection of stator winding inter-turn fault for pm synchronous motor drives," in *2007 IEEE Vehicle Power and Propulsion Conference*, pp. 95–100, Sept 2007.

[35] J. Faiz, H. Nejadi-Koti, and Z. Valipour, "Comprehensive review on inter-turn fault indexes in permanent magnet motors," *IET Electric Power Applications*, vol. 11, no. 1, pp. 142–156, 2017.

[36] A. Ferrero and G. Superti-Furga, "A new approach to the definition of power components in three-phase systems under nonsinusoidal conditions," *IEEE Trans. on Instrumentation and Measurement*, vol. 40, no. 3, pp. 568–577, 1991.

APPENDIX A

SPECIFICS OF PMSM IN EXPERIMENT

This appendix displays the specific of PMSM used in the simulation and experiment.

Table A.1: Specifics of PMSM in experiment

rating voltage	220 V
rating torque	4 N*m
maximum torque	12 N*m
rating speed	2500 rpm
line resistance	2.75 Ω
line inductance	7 mH
rating power	1 KW
phase current	4 A
emf constant	0.087 V/(rad/s)
Inertia	$0.85 * 10^{-3} Kg * m^2$

APPENDIX B

CLOSED-FORM SOLUTION OF i_0

This appendix displays the closed-form solution of i_0. And it is also used to calculate i_0 in the controller in simulation and experiment.

Define:

$$K1 = -\frac{3}{\mu_{sc}} \tag{B.1}$$

$$K2 = L_{as2} + M_{a1a2} - \mu_{sc}M \tag{B.2}$$

$$K3 = K1(r_f + R_a2) + 2R_a2 \tag{B.3}$$

$$K4 = \omega_e(K1L_{as2} + 2K2) \tag{B.4}$$

$$K5 = i_{sq}R_a2 + \mu_{sc}K_{emf}\omega_e \tag{B.5}$$

$$K6 = K2i_{sq}\omega_e \tag{B.6}$$

Then:

$$I_0 = K1\frac{\sqrt{K5^2 + K6^2}}{\sqrt{K3^2 + K4^2}} \tag{B.7}$$

$$\varphi_0 = arctan(\frac{K6}{K5}) - arctan(\frac{K4}{K3}) \tag{B.8}$$

SC EFFECT ON INDUCTANCE

This appendix explains how to determine the self-inductance given certain ratio. This PMSM is the one used in experiment.

Fig. C.1 shows the coils connection of one phase winding in PMSM with 4 pole pairs. Each coil represents coils per pole pair.
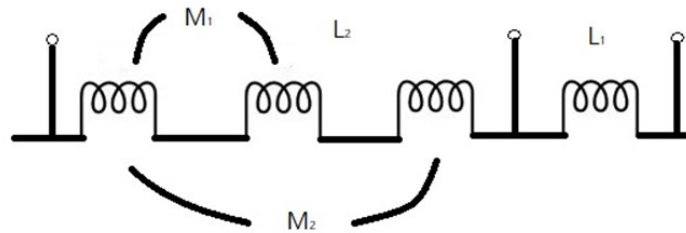
Figure C.1: Coils connection of one phase winding

Based on measurements and calculation:

$$L_s = 0.75mH \tag{C.1}$$

$$M_1 = 0.045mH \tag{C.2}$$

$$M_2 = -0.105mH \tag{C.3}$$

The PMSM in experiment has 12 coils (P=12).

Fig. C.2 shows the coils connection per pole pair per phase.
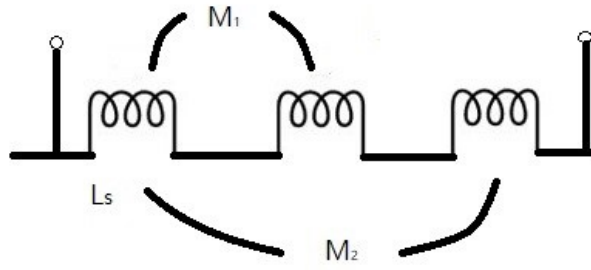
Figure C.2: Coils connection per pole pair per phase

Based on measurements and calculation:

$$L_s = 0.57mH \tag{C.4}$$

$$M_1 = -0.395mH \tag{C.5}$$

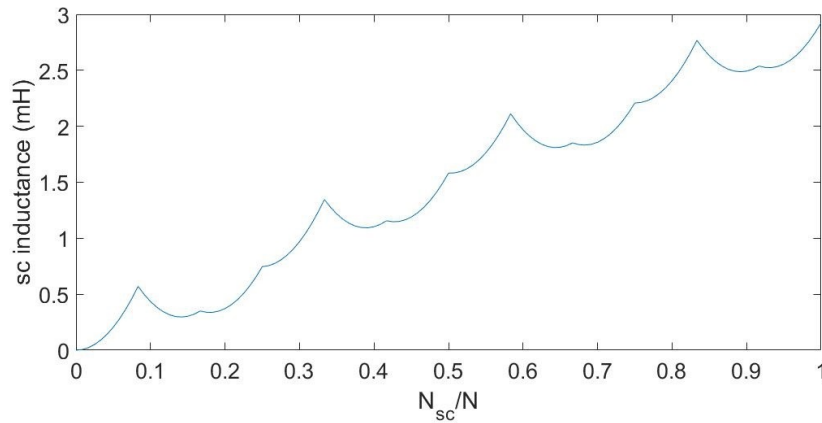$$M_2 = 0.308mH \tag{C.6}$$

Fig. C.3 shows the self inductance with SC.

Figure C.3: Winding inductance with SC

As for self-inductance, following expression can be used.

$$M_{a1a2} = \frac{L - L_{a1} - L_{a2}}{2} \tag{C.7}$$
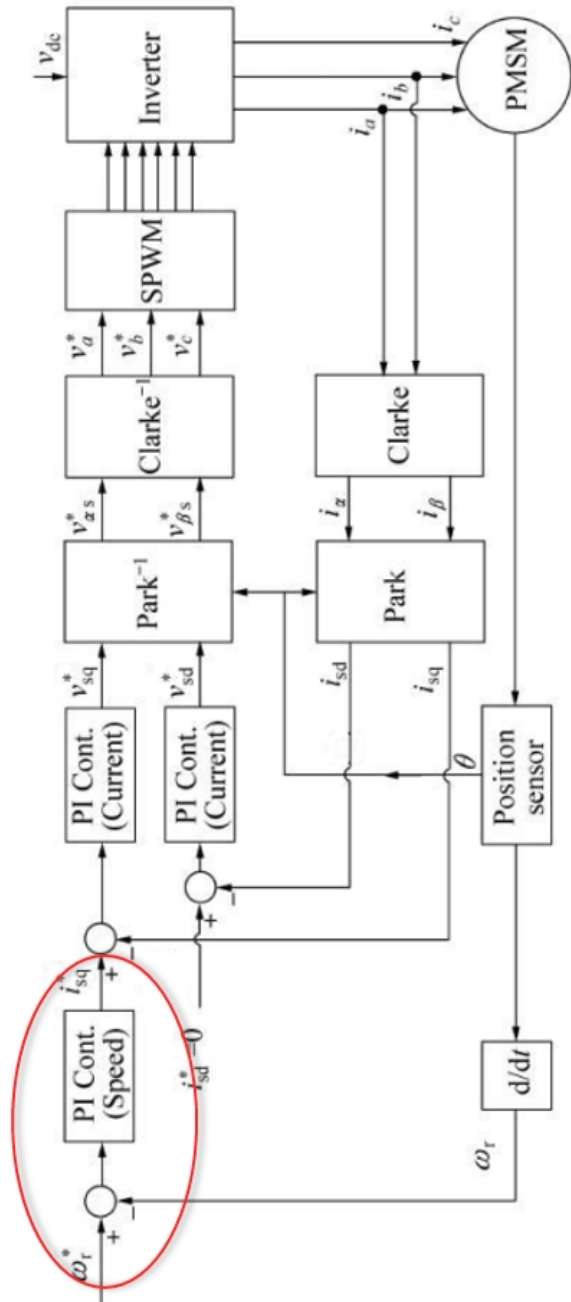
APPENDIX D

FOC SCHEME

Next page shows the FOC scheme.

Figure D.1: FOC scheme

APPENDIX E
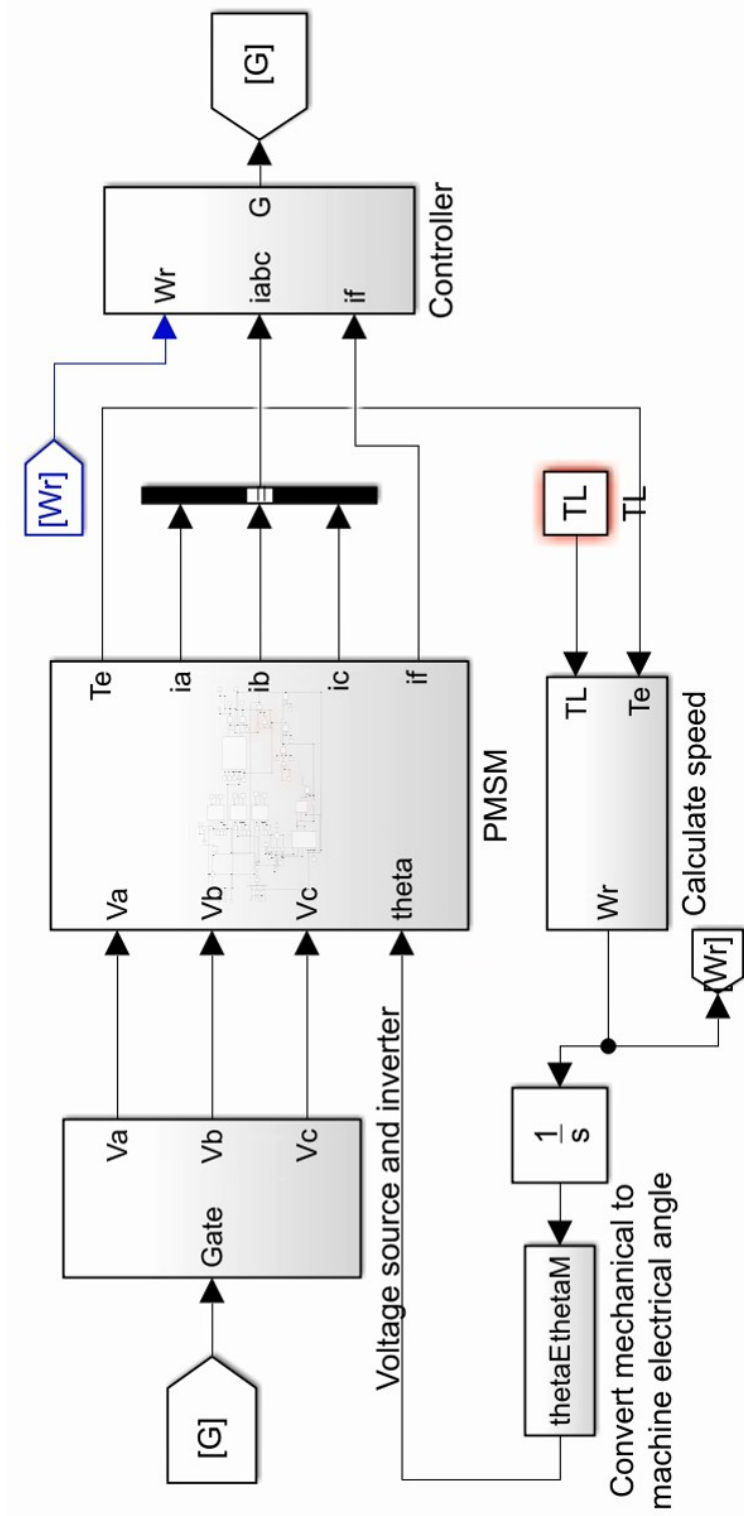
SIMULATION SETUP

Next page shows the simulation setup.

Figure E.1: Simulation setup

APPENDIX F

HARDWARE INFORMATION
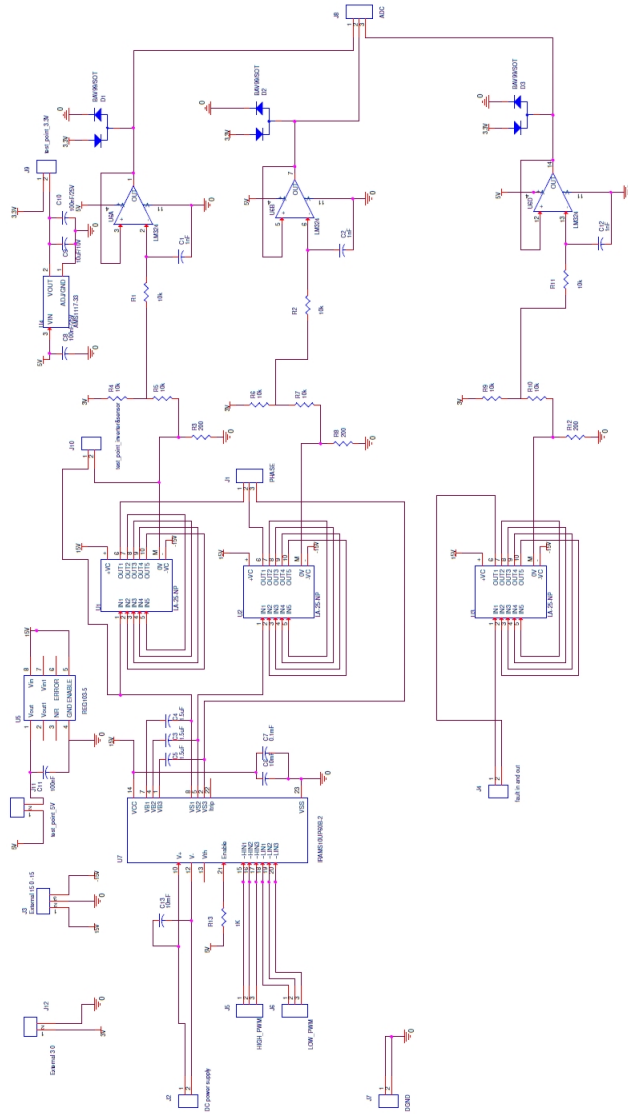

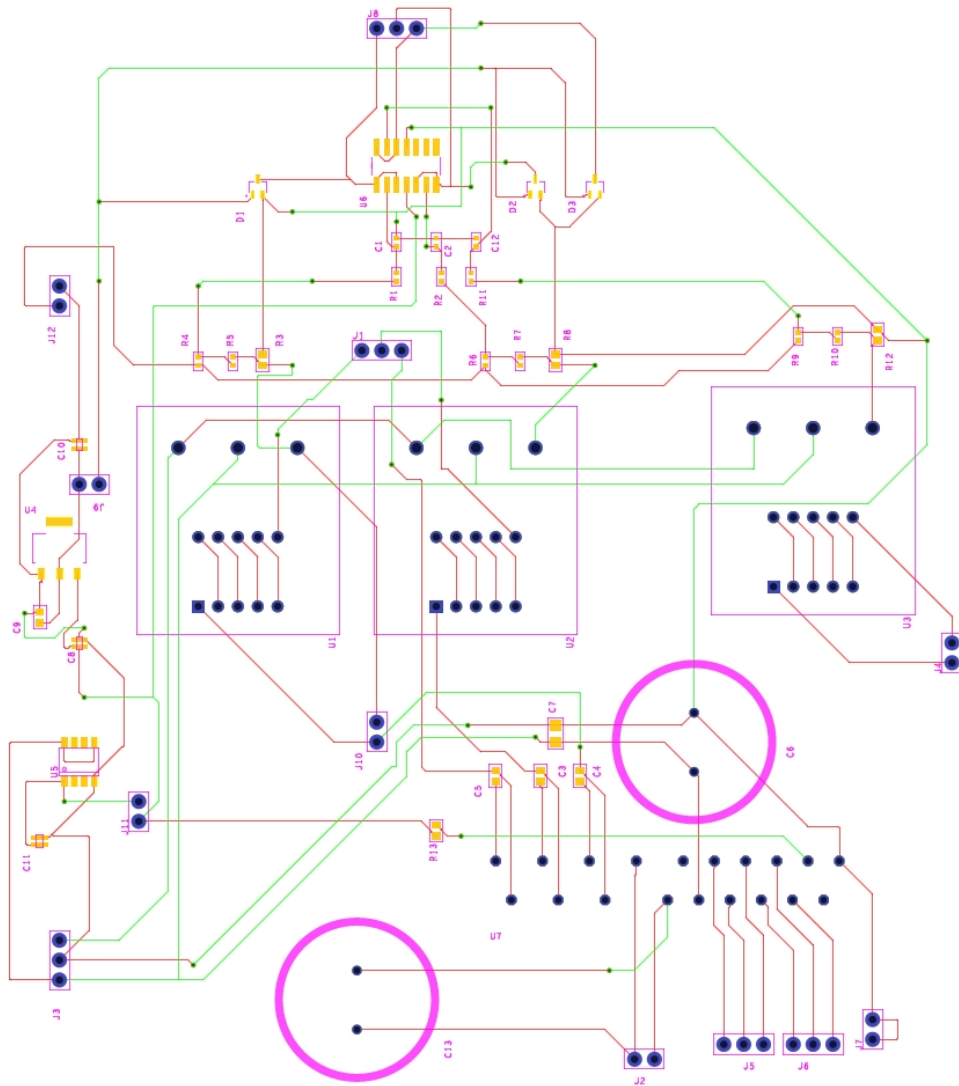Following pages show PCB schematics and PCB layout.

Figure F.1: Schematics of PCB

Figure F.2: PCB layout